UC San Diego
UC San Diego Previously Published Works

Title

Calcium signals regulate the functional differentiation of thymic iNKT cells

Permalink
https://escholarship.org/uc/item/7sf0q2h4

Journal
The EMBO Journal, 40(16)

ISSN
0261-4189

Authors
Zhao, Meng
Quintana, Ariel
Zhang, Chen
et al.

Publication Date
2021-08-16

DOI
10.15252/embj.2021107901

Peer reviewed

eScholarship.org Powered by the California Digital Library
University of California

Article

TRANSPARENT PROCESS

THE EMBO JOURNAL

Calcium signals regulate the functional differentiation of thymic iNKT cells

Meng Zhao[1,2,3,*,†,‡], Ariel Quintana[4,5,†], Chen Zhang[4,†], Alexander Y Andreyev[6,†], William Kiosses[7], Tomomi Kuwana[8], Anne Murphy[9], Patrick G Hogan[4,10,**,‡] & Mitchell Kronenberg[1,11,***,‡]

Abstract

How natural or innate-like lymphocytes generate the capacity to produce IL-4 and other cytokines characteristic of type 2 immunity remains unknown. Invariant natural killer T (iNKT) cells differentiate in the thymus into NKT1, NKT2, and NKT17 subsets, similar to mature, peripheral CD4$^+$ T helper cells. The mechanism for this differentiation was not fully understood. Here, we show that NKT2 cells required higher and prolonged calcium (Ca^{2+}) signals and continuing activity of the calcium release-activated calcium (CRAC) channel, than their NKT1 counterparts. The sustained Ca^{2+} entry via CRAC pathway in NKT2 cells was apparently mediated by ORAI and controlled in part by the large mitochondrial Ca^{2+} uptake. Unique properties of mitochondria in NKT2 cells, including high activity of oxidative phosphorylation, may regulate mitochondrial Ca^{2+} buffering in NKT2 cells. In addition, the low Ca^{2+} extrusion rate may also contribute to the higher Ca^{2+} level in NKT2 cells. Altogether, we identified ORAI-dependent Ca^{2+} signaling connected with mitochondria and cellular metabolism, as a central regulatory pathway for the differentiation of NKT2 cells.

Keywords calcium signaling; iNKT cells; metabolism; mitochondria; T-cell differentiation

Subject Categories Immunology; Signal Transduction

DOI 10.15252/embj.2021107901 | Received 1 February 2021 | Revised 20 May 2021 | Accepted 25 May 2021 | Published online 25 June 2021

The EMBO Journal (2021) 40: e107901

Introduction

Invariant natural killer T (iNKT) cells are a group of innate-like T lymphocytes. They are distinguishable from mainstream CD4$^+$ and CD8$^+$ T cells by many features, including the expression of the semi-invariant T-cell receptors (TCRs), restriction by the non-polymorphic MHC-class I-like molecule CD1d, specificity for lipid antigens, tissue residency, and, importantly, their rapid effector functions upon activation (Kronenberg, 2005; Godfrey *et al*, 2010; Brennan *et al*, 2013). Unlike mainstream T cells, which undergo activation and proliferation in the periphery before differentiating into effector T cells with defined profiles of cytokine production, iNKT cells differentiate during thymic development into functional subsets, NKT1, NKT2, and NKT17, analogous to Th1, Th2, and Th17 CD4$^+$ helper T lymphocytes. The subsets differ for the expression of hundreds of genes (Engel *et al*, 2016; Georgiev *et al*, 2016; Lee *et al*, 2016). Several transcription factors and cytokines have been shown to influence the prevalence of the iNKT cell subsets (Salio *et al*, 2014; Krovi & Gapin, 2018). The selective activation of these subsets could be the mediators for the divergent effects of the total population of iNKT cells, which are in some situations anti-inflammatory, while in others pro-inflammatory (Kronenberg, 2005; Wang *et al*, 2018; Zhao *et al*, 2018). For example, recently IFNγ-producing NKT1 cells were shown to be important in preventing severe disease in an autoimmune arthritis model (Zhao *et al*, 2018). Therefore, despite their similar TCRs and specificity, iNKT cell subsets represent lymphocytes that physiologically are highly different.

It has been shown that thymic iNKT cells have many important functions. In particular, thymic NKT2 cells are a major IL-4 producer at steady state, which has striking consequences for the homeostasis of thymic cell populations (Lee *et al*, 2013; Kang *et al*,

1 Division of Developmental Immunology, La Jolla Institute for Immunology, La Jolla, CA, USA
2 Arthritis and Clinical Immunology Program, Oklahoma Medical Research Foundation, Oklahoma City, OK, USA
3 Department of Microbiology and Immunology, University of Oklahoma Health Science Center, Oklahoma City, OK, USA
4 Division of Signaling and Gene Expression, La Jolla Institute for Immunology, La Jolla, CA, USA
5 Translational Science Division, Clinical Science Department, Moffitt Cancer Center Magnolia Campus, Tampa, FL, USA
6 Department of Molecular Medicine, The Scripps Research Institute, La Jolla, CA, USA
7 Core Microscopy, La Jolla Institute for Immunology, La Jolla, CA, USA
8 Division of Immune Regulation, La Jolla Institute for Immunology, La Jolla, CA, USA
9 Cytokinetics, South San Francisco, CA, USA
10 Moores Cancer Center, University of California San Diego, La Jolla, CA, USA
11 Division of Biological Sciences, University of California, San Diego, La Jolla, CA, USA
*Corresponding author. Tel: +1 405 2717905; E-mail: meng-zhao@omrf.org
**Corresponding author. Tel: +1 858 9527175; E-mail: phogan@lji.org
**Corresponding author. Tel: +1 858 752 6540; E-mail: mitch@lji.org
†These authors contributed equally to this work
‡These authors contributed equally to this work as senior authors

© 2021 The Authors

2016). The development of iNKT cells in the thymus requires a stronger signal than required for mainstream $CD4^+$ or $CD8^+$ T cells, a process also known as agonist-mediated positive selection (Baldwin *et al*, 2004; Cheroutre *et al*, 2009). We and others have recently shown that TCR signaling strength regulates the differentiation of iNKT cell subsets; and NKT2 cells require optimal zeta chain of TCR-associated protein kinase 70 (Zap70)-mediated signals (Tuttle *et al*, 2018; Zhao *et al*, 2018), which is consistent with the higher expression level of Nur77 reporter (Moran *et al*, 2011; Lee *et al*, 2013) in mature NKT2 cells.

Engagement of the TCR causes phosphorylation of phospholipase C (PLC), which hydrolyzes phosphatidylinositol 4,5 bisphosphate (PIP_2) to inositol 1,4,5 trisphosphate ($InsP_3$) and diacylglycerol (DAG; Courtney *et al*, 2018). $InsP_3$ releases calcium (Ca^{2+}) from the endoplasmic reticulum (ER) intracellular Ca^{2+} stores, causing the activation of Ca^{2+} release-activated Ca^{2+} (CRAC)/ORAI channels through the stromal interaction molecule (STIM; Hogan & Rao, 2015; Bird & Putney, 2018; Ong *et al*, 2019). The development of iNKT cells and other agonist-selected T cells requires STIM-ORAI Ca^{2+} signaling (Oh-Hora *et al*, 2013). In contrast, mainstream or conventional thymocytes can develop but are hypo-responsive in the absence of CRAC/ORAI function. Downstream of Ca^{2+} entry, the calcineurin-nuclear factor of activated T-cell (NFAT) pathway is particularly important for iNKT cell differentiation, as is early growth response 2 (Egr2), a transcription factor regulated by NFAT (Shao *et al*, 1997; Rengarajan *et al*, 2000; Lazarevic *et al*, 2009). Egr2 directly regulates pro-myelocytic leukemia zinc finger (PLZF) expression in iNKT cells (Seiler *et al*, 2012), which is important for their acquisition of effector functions (Kovalovsky *et al*, 2008; Savage *et al*, 2008). NKT2 cells express higher amount of Egr2 (Georgiev *et al*, 2016) and PLZF (Engel *et al*, 2016), in line with the influence of stronger TCR signals in driving this subset. Nevertheless, it is unknown whether Ca^{2+} signaling is differentially regulated in thymic iNKT cell subsets and whether processes related to the intracellular Ca^{2+} homeostasis are important for subset differentiation.

Apart from acting in the cytoplasm, Ca^{2+} is taken up by mitochondria and regulates the activity of oxidative phosphorylation, the main pathway for ATP production in naïve T cells (Contreras *et al*, 2010; van der Windt & Pearce, 2012). The differentiation of iNKT cells to acquire effector function is bioenergetically demanding (Pearce *et al*, 2013). The extent to which thymic iNKT cells are metabolically distinct from the mainstream thymic T cells remains to be fully characterized. However, deletion of genes encoding metabolic regulators such as c-Myc, and Raptor (Mycko *et al*, 2009; Zhang *et al*, 2014) specifically abolished iNKT cell development, but not conventional T cells. Furthermore, a recent study showed that knocking out Uqcrfs1, the gene encoding an essential subunit of mitochondrial respiratory chain complex III, RISP, also resulted in a diminished iNKT cell compartment without affecting the development of conventional T cells, indicating that oxidative phosphorylation is essential for iNKT cell development. It remains to be determined, however, how metabolic regulation differentially controls the development of the iNKT cell subsets, but Rictor deletion has been implicated as a requirement for NKT2 cells (Prevot *et al*, 2015).

In this study, we showed that the two most abundant subsets, thymic NKT1 and NKT2 cells, display distinct intracellular Ca^{2+} homeostasis downstream of TCR activation and have a different requirement of Ca^{2+} for proliferation and differentiation. Furthermore, thymic iNKT cells have significantly higher ATP demand, and uniquely active mitochondria respiration, as compared to conventional T cells. We also showed that BTP2, a CRAC channel inhibitor abolishes Ca^{2+} influx downstream of TCR in NKT2 cells, and further dampens their development. Furthermore, mitochondria in NKT2 cells not only exhibited a structural basis for high oxidative phosphorylation in these cells, but also played a role in regulating Ca^{2+} signaling in NKT2 cells.

Results

Different Ca^{2+} influx in activated iNKT cell subsets

We have recently shown that NKT2 cells required optimal TCR signals to develop, whereas NKT1 cells differentiated even when TCR signals were reduced due to two different hypomorphic Zap70 mutations (Zhao *et al*, 2018). In addition, we found that mRNA expression of genes that regulate TCR signal transduction is significantly different in iNKT cell subsets (Zhao *et al*, 2018), suggesting that their TCR signaling pathways are controlled differentially. One of the early signaling cascade triggered upon TCR activation is the rise of intracellular Ca^{2+} as a result of Ca^{2+} influx through plasma membrane Ca^{2+} channels. We monitored Ca^{2+} influx after TCR activation using flow cytometry (Fig 1A), gating on the two major thymic subsets of CD1d tetramer$^+$ iNKT cells: NKT1 ($ICOS^{lo}CD4^{+/-}$) and NKT2 ($ICOS^{hi}CD4^+$), after iNKT cell enrichment by negative selection. Ratiometric dye Indo-1 was used to report cytoplasmic Ca^{2+} concentration ($[Ca^{2+}]$) (Bailey & Macardle, 2006). Antibody cross-linker (goat anti-Armenian hamster IgG (H + L)) was added in the absence of extracellular Ca^2. Upon addition of 1mM Ca^{2+} solution, cytoplasmic Ca^{2+} rapidly and transiently increased as a result of TCR signaling-induced Ca^{2+} influx. There are number of differences, but importantly, the maximal cytoplasmic $[Ca^{2+}]$ was higher in NKT2 cells, and the cytoplasmic $[Ca^{2+}]$ was sustained at a higher level in NKT2 cells during the analysis (Fig 1A). To assess the heterogeneity of these thymic populations, we carried out single-cell Ca^{2+} imaging, as published previously (Sharma *et al*, 2013). Freshly sorted thymic NKT1 and NKT2 cells were labeled with Fura-2, another ratiometric fluorescent Ca^{2+} indicator (Grynkiewicz *et al*, 1985), stimulated with anti-CD3ε and anti-CD28 antibodies in the absence of extracellular Ca^{2+}, and Ca^{2+} influx was observed upon 1mM Ca^{2+} perfusion (Fig 1B, Appendix Fig S1A and B). This analysis confirmed the higher maximal Ca^{2+} signals, and more sustained Ca^{2+} increase in NKT2 cells than in NKT1 cells. While the magnitude of the NKT1-NKT2 divergence was different in the two assays, and there was some overlap for the maximal cytoplasmic Ca^{2+} in the single-cell analysis (Appendix Fig S1C), the data clearly indicate the two populations can be distinguished by maximal and sustained Ca^{2+} influx (Fig 1B and Appendix Fig S1C). Therefore, TCR activation induced a higher and more prolonged Ca^{2+} signal in differentiated thymic NKT2 cells.

We next analyzed thymus iNKT cell subsets from SKG mice, which have a hypomorphic mutation in *Zap70*. Using Indo-1 and flow cytometry-based assay of cell populations, SKG NKT1 cells exhibited a similar cytoplasmic Ca^{2+} profile upon TCR activation as compared to WT NKT1 cells (Fig 1C), whereas in SKG NKT2 cells, the maximal Ca^{2+} level was significantly reduced compared with

 © 2021 The Authors

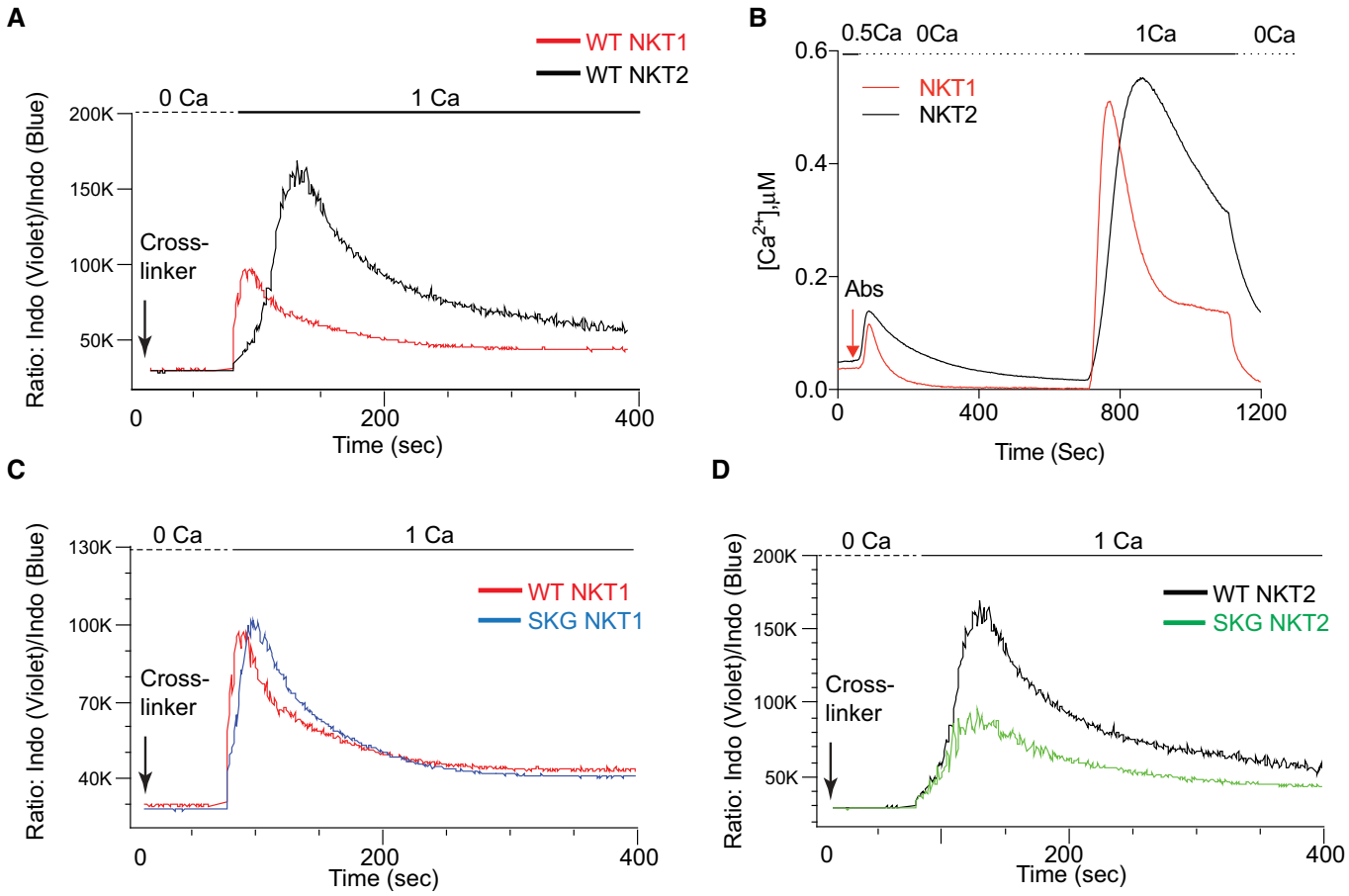

Figure 1. Distinct Ca^{2+} influx in thymic iNKT cell subsets.

A Population analysis. Pre-enriched iNKT cells from WT BALB/c mice (NKT1, Red; NKT2, Black) were stained with Indo-1. As a measure of intracellular [Ca^{2+}], the ratio of Indo (Violet) and Indo (Blue) was analyzed by flow cytometry. Timing of the addition of cross-linker, goat anti-Armenian hamster IgG (H + L), and extracellular calcium (mM) was as indicated.

B Single-cell analysis. Average profiles of Ca^{2+} influx induced by anti-CD3ε, and anti-CD28 in freshly sorted individual NKT1 (Red) and NKT2 (Black) cells, labeled by Fura-2. The average signal from more than 200 cells is shown. The timing of antibody addition, and the extracellular [Ca^{2+}] are indicated (mM).

C, D Pre-enriched thymocytes from WT BALB/c thymi as in (A) were labeled by CFSE ($CFSE^{+}$), mixed with pre-enriched thymocytes from SKG thymi ($CFSE^{-}$), loaded with Indo-1, and stimulated as in (A). Ratio of Indo (Violet) and Indo (Blue) was analyzed by flow cytometry. Comparison of cytoplasmic Ca^{2+} profiles between WT and SKG NKT1 (C) and NKT2 (D) cells in the same test tube are shown. Data are representative from one of at least three independent experiments. Graphs represent the average Ca^{2+} levels.

WT NKT2 cells (Fig 1D). Because NKT2 cell differentiation is impaired in SKG mice due to *Zap70* mutation (Zhao *et al*, 2018), these data indicate that differential regulation of Ca^{2+} homeostasis downstream of ZAP70 may be important for subset differentiation, or related to the accumulation of differentiated NKT2 cells, for example by increasing proliferation.

Higher Ca^{2+} is required for TCR-induced NKT2 proliferation

Because the specific TCR α gene rearrangement that commits cells to the iNKT cell lineage is infrequent, iNKT cells must undergo intra-thymic proliferation to generate the populations of 5×10^5 or more mature iNKT cells that are typically observed in young adult mouse thymus. Ca^{2+} signals regulate cell proliferation (Rodrigues *et al*, 2007), and therefore, we compared TCR-induced proliferation in vitro using sorted NKT1 and NKT2 thymocytes. NKT2 cells were more proliferative (Fig 2A), consistent with transcriptomic analysis (Engel *et al*, 2016). To examine the requirement for extracellular Ca^{2+} for proliferation, EGTA was added to Ca^{2+}-free DMEM culture medium. The Ca^{2+} in the medium comes from the FBS supplement. In order to measure effects on proliferation accurately, aside from effects on cell survival, we monitored the survival rate of iNKT cell subsets in the presence of different EGTA concentrations. At 0.45 mM EGTA, the percentage of live cells was significantly reduced for both iNKT cell subsets, whereas there was no effect at 0.40 mM and lower concentrations (Appendix Fig S2). Importantly, EGTA inhibited NKT2 cell proliferation in a dose-dependent manner at concentrations where cell viability was not reduced, whereas NKT1 cell proliferation was maintained (Fig 2A and B). To test for the Ca^{2+} dependence of NKT1 and NKT2 cell proliferation without

© 2021 The Authors

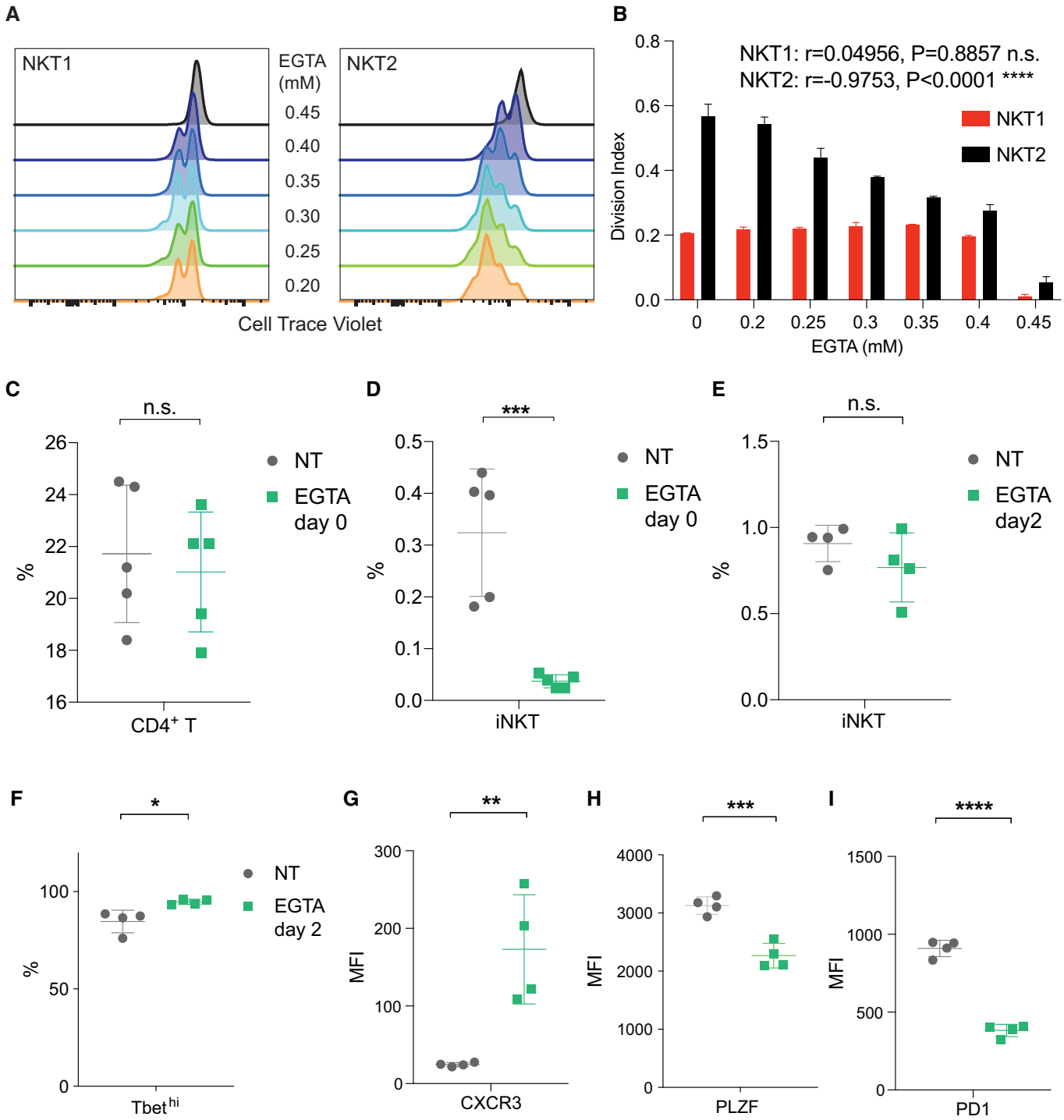

Figure 2. NKT2 cells require more Ca^{2+} for proliferation and differentiation.

A Sorted thymic NKT1 and NKT2 cells were labeled with CellTrace Violet, and activated by anti-CD3ε/CD28 Dynabeads for 2 days, in the presence of different [EGTA] in the medium. CellTrace Violet/CTV signal in living cells at the end of the culture is shown.

B Cell proliferation was quantified as division index based on CTV signals in (A).

C–I Thymic lobes from new born (day 0) BALB/c mice were cultured in vitro for 6 days. (C, D) EGTA was added from the start of culture (day 0), and the percentages of $CD4^+$ T cells (C) and iNKT cells (D) among live cells are shown. (E–I) EGTA was added 48 h after the start of culture (day 2), and the percentage of iNKT cells (E), the percentage of $Tbet^{hi}$ population in iNKT cells (F), and the expression of CXCR3 (G), PLZF (H), and PD1 (I) in total iNKT cells are shown.

Data information: Data are representative from one of at least three independent experiments. Graphs represent mean ± SD with three replicate samples (B) or symbols representing individual thymic lobes (C–I). For (B), ****$P < 0.0001$; n.s. not significant (nonparametric Spearman correlation between division index and EGTA concentration); For (C–I), *$P < 0.05$; **$P < 0.01$; ***$P < 0.001$; ****$P < 0.0001$; n.s. not significant (unpaired two-tailed Student's *t*-test).

 © 2021 The Authors

EGTA, we dialyzed FBS against Ca^{2+}-free DMEM to reduce the Ca^{2+} concentration in the medium and added known amounts of $CaCl_2$. We found that while cell survival was not affected (Appendix Fig S3A), increasing Ca^{2+} promoted NKT2 cell proliferation in a dose-dependent fashion up to at least 0.4 mM, whereas NKT1 cell proliferation was not sensitive to Ca^{2+} changes (Appendix Fig S3B). Collectively, these data show that increased Ca^{2+} availability upon TCR triggering was required for optimal NKT2 cell proliferation.

NKT2 differentiation is sensitive to Ca^{2+} chelation

We have established a fetal thymic organ culture (FTOC) system that not only recapitulates the early events during iNKT cell ontogeny but provides for the differentiation of functional iNKT cell subsets (Zhao *et al*, 2018). To examine further the role of Ca^{2+} during subset differentiation, EGTA (1 mM) was added at different times to the FTOC. The development of iNKT cells was abolished by day 0 addition of EGTA, whereas conventional $CD4^+$ and $CD8^+$ T cells were not affected (Fig 2C and D, Appendix Fig S4A). This shows that iNKT cells required higher Ca^{2+} signals to develop. In the FTOC, iNKT cells emerged at the third day of culture (Zhao *et al*, 2018). When EGTA was added at 48 h (day 2), the total number of iNKT cells was not reduced (Fig 2E), suggesting that optimal Ca^{2+} is necessary during the early commitment to become an iNKT cell, but less so during their subsequent expansion and further differentiation. However, when examining the subsets arising after day 2 EGTA addition, the NKT1 population ($Tbet^{hi}$) was increased, together with higher expression of NKT1 markers CXCR3 and CD122 (Fig 2F and G; Appendix Fig S4B). In contrast, the NKT2 cell population was reduced, as evidenced by lower expression of NKT2 markers PLZF, PD1, and Slamf6 (Fig 2H and I; Appendix Fig S4C). The reciprocal increase in NKT1 and decrease in NKT2 cells is most consistent with the hypothesis that continued and optimal Ca^{2+} is critical for NKT2 cell differentiation.

NKT2 cells are metabolically active

Consistent with higher proliferative capacity of NKT2 cells, RNA-seq analysis comparing thymic NKT1 and NKT2 cells from WT BALB/c mice indicated that pathways related to cell cycle regulation showed significant enrichment in NKT2 cells, as well as biosynthesis pathways for nucleotides and amino acids, building blocks for DNA, RNA, and protein (Fig 3A). Interestingly, genes related to oxidative phosphorylation, mitochondrial function, and glycolysis were also enriched in NKT2 cells suggesting that they are more metabolically active. Compared with $CD4^+$ T cells from the thymus, we found NKT1 and NKT2 cells had a higher ATP level per cell, with NKT2 cells having the highest ATP content of any of the mature thymocyte populations tested (Fig 3B). Flow cytometry analysis indicated NKT2 cells are larger, but when corrected for cell size, NKT2 cells still had a higher ATP concentration (Appendix Fig S5).

Naïve T cells depend on mitochondrial oxidative phosphorylation to generate ATP (Pearce *et al*, 2013). Mitochondrial Ca^{2+} uptake stimulates the aerobic synthesis of ATP through the activation of the pyruvate, α-ketoglutarate, and isocitrate dehydrogenases (Contreras *et al*, 2010). Thus, we hypothesized that Ca^{2+}-dependent mitochondrial function was distinctively important for NKT2 cells. To directly test the activity of mitochondrial respiration, we carried out the Mito Stress test using the Seahorse instrument (Fig 3C). We measured metabolic parameters such as basal and maximal oxidative phosphorylation, glycolysis, and ATP demand as described in Appendix Fig S6. The oxygen consumption rate (OCR) is a specific measurement of mitochondrial activity. The higher basal OCR in NKT2 cells than in NKT1 and $CD4^+$ T cells from the thymus is indicative of higher mitochondrial respiration at steady state (Fig 3D). Spare respiratory capacity (SRC) is an indicator of the respiratory potential available to a cell to produce energy under stress. NKT1 and NKT2 cells had a higher SRC than mainstream, mature thymocytes (Fig 3E). NKT2 cells specifically had the highest basal/maximal/spare respiration among all mature thymic T populations tested, indicating that mitochondria in NKT2 cells are particularly active (Fig 3D, Appendix Fig S7A, Fig 3E). The extracellular acidification rate (ECAR, Appendix Fig S7B) measures pH changes in the microwell and reflects the rate of lactate production from glucose, as well as carbon dioxide production from glycolytically produced pyruvate (CO_2 dissolved in the medium). In the presence of oligomycin, however, mitochondrial ATP synthesis, and consequently, respiration and pyruvate utilization are suppressed nearly completely (so-called respiratory control). This is evident from almost no difference between OCRs in the presence of oligomycin versus respiratory inhibitor myxothiazol (Fig 3C, Appendix Fig S6A). As no CO_2 is produced in this case, the ECAR reports exclusively lactic acid production/glycolic activity. This activity reflects maximal capacity of glycolysis to respond to the basal ATP demand of the cells (Fig 3F, Appendix Fig S6). We calculated (using approach described in Appendix Fig S6) that these maximal capacities can meet only between 20% (NKT1) and 40% (NKT2) of the total ATP demand (Appendix Fig S7C) of the cell. Thus, both types of iNKT cells, as well as T cells, are critically dependent on oxidative phosphorylation for energy (Appendix Fig S7D), although NKT2 cells are capable of higher, albeit transient, glycolytic activity than other T cells (Appendix Fig S7B). Also, by subtracting ECAR readings in glucose-free medium (supplemented with pyruvate and glutamine to provide substrate for mitochondria, Appendix Fig S6), we were able to determine the relative contribution of glycolysis to bioenergetics of T cells under basal conditions and demonstrated that NKT2 cells have higher spare glycolytic capacity (Fig 3F and G), while NKT1 cells are more similar to other mature CD4 and CD8 thymocytes. Overall, metabolism of NKT2 cells is uniquely high among tested thymocytes. The total basal ATP demand, measured as the combination of basal ATP production from oxidative phosphorylation and glycolysis (Appendix Fig S6), in iNKT cells, especially NKT2 cells, is significantly higher than in conventional $CD4^+$ and $CD8^+$ T cells (Appendix Fig S7C). The vast majority of the ATP demand is met by oxidative phosphorylation in all thymocyte populations tested (Appendix Fig S7D). The higher ATP production in iNKT cells may be critical to meet the bioenergetic demand for effector functions, such as iNKT cell IL-4 production at steady state that affects other thymocytes (Lee *et al*, 2013; Miller *et al*, 2018).

Mitochondria reflect activities of oxidative phosphorylation in iNKT cell subsets

The vast majority of mitochondrial proteins are encoded by nuclear genes and are transported from the cytosol to mitochondria via protein import machinery (Pfanner *et al*, 2019). Several translocases

© 2021 The Authors

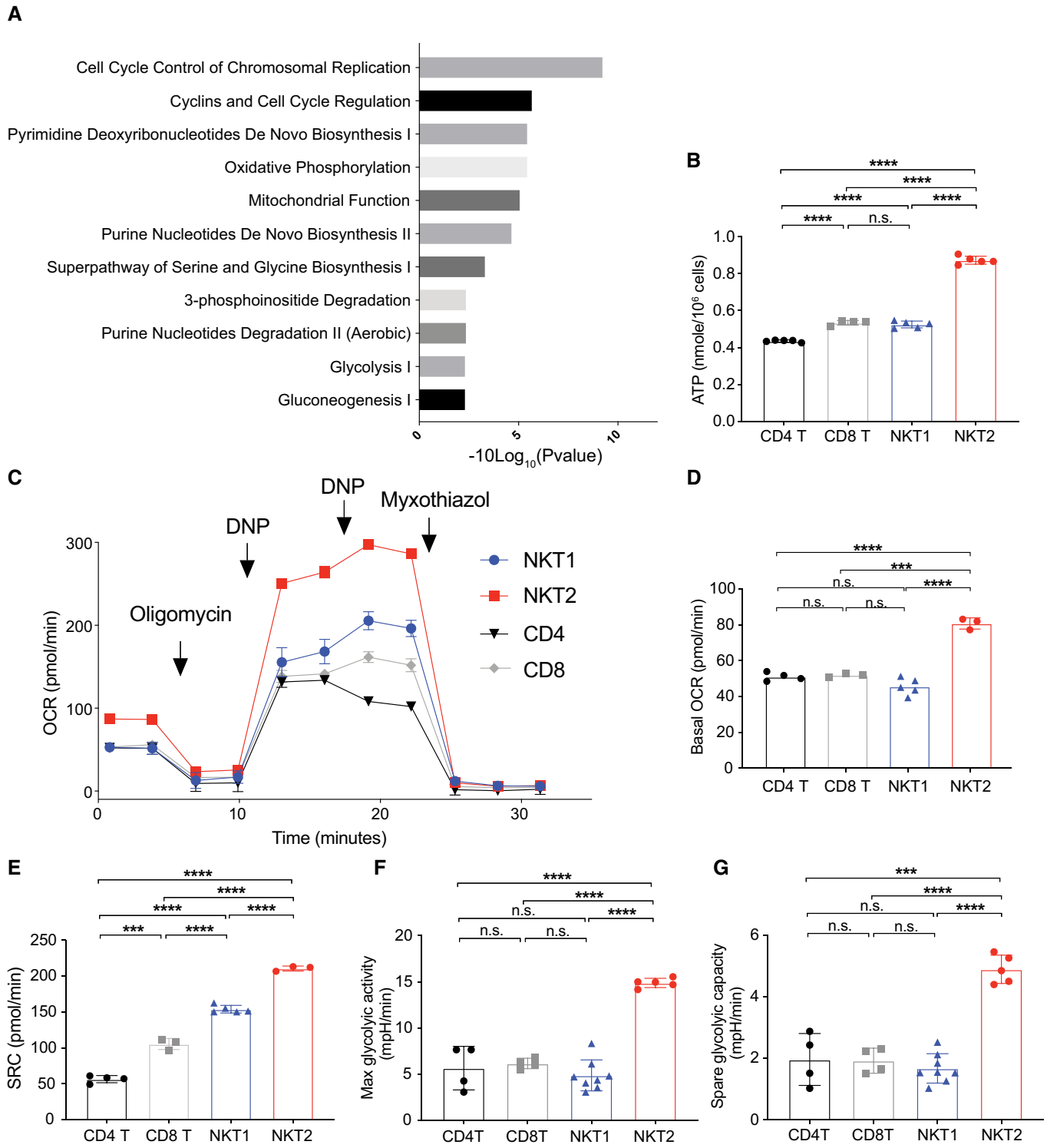

Figure 3. NKT2 cells are more metabolically active.

A Enriched pathways comparing BALB/c thymic NKT1 and NKT2 transcriptomes.
B ATP content from sorted thymic T-cell populations.
C Oxygen consumption rate (OCR) from sorted thymic T-cell populations measured in a Seahorse Mitostress test.
D, E (D) basal OCR and (E) spare respiratory capacity (SRC) were calculated based on data from (C).
F, G (F) maximal glycolytic activity and (G) spare glycolytic capacity were calculated as in Appendix Fig S6.

Data information: Data are representative from one of at least three independent experiments. Graphs represent mean ± SD with symbols representing individual samples. ***$P < 0.001$; ****$P < 0.0001$; n.s. not significant (unpaired two-tailed Student's *t*-test).

 © 2021 The Authors

of the outer membrane (TOM), Tomm20 and Tomm40, and translocases of the inner membrane (TIM), Timm8a1 and Timm9, were expressed significantly higher in NKT2 cells than in NKT1 cells based on mRNA levels (Appendix Fig S8A). Although a minor fraction of mitochondrial proteins, a few proteins, including key components in the electron transport chain, are encoded by the mitochondrial DNA (mtDNA) and are translated in mitochondria (Johnston & Williams, 2016). All the differentially expressed genes encoding mitochondrial ribosomal proteins were expressed at higher level in NKT2 cells than in NKT1 cells, including mitochondrial ribosomal proteins S6 (encoded by *Mrps6*), S28 (*Mrps28*), L54 (*Mrpl54*), and L34 (*Mrpl34*). Similarly, *Gfm1* and *Gfm2* encoding mitochondrial elongation factors G1 and G2, and *Mrrf* encoding mitochondrial ribosome recycling factor, were also expressed higher in NKT2 cells. Consistent with the higher expression of genes encoding mitochondrial proteins (Appendix Fig S8A) and higher level of oxidative phosphorylation (Fig 3), MitoTracker green staining showed that the mitochondrial mass was increased in NKT2 compared with NKT1 cells (Fig 4A and B). 3D confocal imaging by staining for Tim23, a key translocase of inner membrane for protein transport, further showed the higher mitochondria volume in NKT2 cells as normalized to total cell volume (Fig 4C and D). Using Stochastic Optical Reconstruction Microscopy (STORM), we were able to measure the number of Tom22 molecules, a mitochondrial outer membrane protein, on a single-cell basis, and found that NKT2 cells expressed a higher amount of Tom22 although there was a similar mRNA level as compared to NKT1 cells (Appendix Fig S8B). Overall, these data indicate that NKT2 cells have higher mitochondria content. Furthermore, electron microscopy (EM) analysis revealed the size of individual mitochondrion in NKT2 cells was significantly larger than in NKT1 cells (Fig 4E and F). Mitochondrial cristae are folds of the inner membrane where oxidative phosphorylation takes place. The cristae length (normalized to individual mitochondria perimeter) in NKT2 cells was significantly higher (Fig 4G). Mitochondrial membrane potential in NKT2 cells was also significantly higher than in NKT1 cells as shown by Tetramethylrhodamine ethyl ester (TMRE) staining (Appendix Fig S8C and D). Therefore, the larger content, together with the morphological and structural features of mitochondria in NKT2 cells, supports the higher oxidative phosphorylation activity and capacity as compared to NKT1 cells in the thymus. MitoTracker green staining also showed that splenic NKT2 cells have higher mitochondria mass than NKT1 cells, suggesting that the differences in mitochondria in thymic subsets may persist in the peripheral organs (Appendix Fig S8E).

CRAC channel is essential for iNKT subsets

Ca^{2+} influx through the STIM-ORAI-dependent calcium release-activated calcium (CRAC) channels is the primary calcium entry pathway downstream of TCR activation in mature T lymphocytes (Hogan & Rao, 2015; Vaeth *et al*, 2020). RNA-seq analysis showed that STIM1, STIM2, ORAI1, ORAI2, and ORAI3 genes were not uniformly expressed at a higher level in NKT2 cells (Appendix Fig S9). To investigate the role of CRAC/ORAI channel activity in iNKT cell subsets, we used BTP2, a CRAC channel inhibitor (Zitt *et al*, 2004; He *et al*, 2005; Steinckwich *et al*, 2007). BTP2 treatment effectively reduced the $[Ca^{2+}]$ peak downstream of TCR activation in NKT1 cells and completely blocked Ca^{2+} influx in NKT2 cells (Fig 5A, Appendix Fig S10A). This suggests that similar to mainstream T cells, the CRAC channel is the predominant Ca^{2+} entry pathway downstream of the TCR in NKT2 cells, and a major Ca^{2+} channel in NKT1 cells, although there may be ORAI-independent Ca^{2+} channels operating in NKT1 cells as well (Fig 5A). A similar effect of BTP2 was also observed in SKG NKT1 and NKT2 cells (Appendix Fig S10B–D).

Given that Ca^{2+} signals are required for NKT2 differentiation (Fig 2), we tested the role of CRAC channels in FTOC. BTP2 treatment in FTOC abolished the development of iNKT cells, but not conventional T cells (Fig 5B, Appendix Fig S10E and F), confirming the previous discovery that the Stim/ORAI pathway is critical for the development of agonist-selected T cells, including iNKT cells (Oh-Hora *et al*, 2013). Delayed addition of BTP2 allowed for a normal percentage of total iNKT cells in FTOC (Appendix Fig S10G–K). However, the differentiation of iNKT cell subsets was skewed toward NKT1 cells, as shown by the increased expression of NKT1 markers CXCR3 and CD122, and the reduced expression of NKT2 markers PLZF, PD1, and Slamf6 (Fig 5C–F, Appendix Fig S10J and K). The similar inhibitory effects of BTP2 and EGTA on iNKT cell differentiation suggest that ORAI channel-mediated Ca^{2+} entry is critical not only for the emergence of iNKT cell precursors, but also for maintaining the essential Ca^{2+} signals required for NKT2 differentiation.

Mitochondria in NKT2 cells regulate store dependent Ca^{2+} signaling

Given the importance of CRAC/ORAI in iNKT cell subset differentiation, we further examined the regulation of CRAC channel activation in iNKT cell subsets. We used single-cell recording and cells were treated with the specific and irreversible sarco/endoplasmic reticulum Ca^{2+}-ATPase (SERCA) blocker thapsigargin (TG) in the absence of extracellular Ca^{2+} in order to induce the full depletion of the ER Ca^{2+} store. The store depletion is the main signal for the activation of CRAC channel; thus, maximal depletion of ER Ca^{2+} stores results in maximal activation of CRAC channels (Prakriya *et al*, 2006). Subsequently, a Ca^{2+}-containing solution (1 mM) was perfused to the extracellular media. The cytoplasmic Ca^{2+} concentration ($[Ca^{2+}]$) quickly increased as a result of Ca^{2+} influx through CRAC channels. WT and SKG iNKT cells had comparable level of the TG-induced Ca^{2+} influx (Fig 6A, Appendix Fig S11C); meanwhile, the addition of BTP2 could inhibit the Ca^{2+} influx process in both cells (Appendix Fig S11). These data indicate that the CRAC channel could function when bypassing the TCR stimulation. Consistent with anti-CD3ε/CD28 stimulation (Fig 1), TG treatment resulted in higher Ca^{2+} in NKT2 cells than in NKT1 cells (Fig 6A and C), suggesting that CRAC channel-mediated Ca^{2+} signaling is regulated differently in NKT2 cells than in NKT1 cells. When $[Ca^{2+}]$ reached a plateau (Fig 6A), extracellular Ca^{2+} removal induced a rapid decrease in the cytoplasmic Ca^{2+} signal likely a result of the halting of Ca^{2+} influx, as well as the Ca^{2+} exportation mechanism at the plasma membrane. After intracellular Ca^{2+} has been reduced to near the baseline level, ionomycin treatment (Fig 6A, blue arrow, Fig 6C) released the remaining Ca^{2+} from intracellular Ca^{2+} stores and increased the cytoplasmic $[Ca^{2+}]$. As TG irreversibly inhibits SERCA pump on ER, the increase in cytoplasmic $[Ca^{2+}]$ after ionomycin is mainly mediated by non-ER Ca^{2+} stores.

© 2021 The Authors

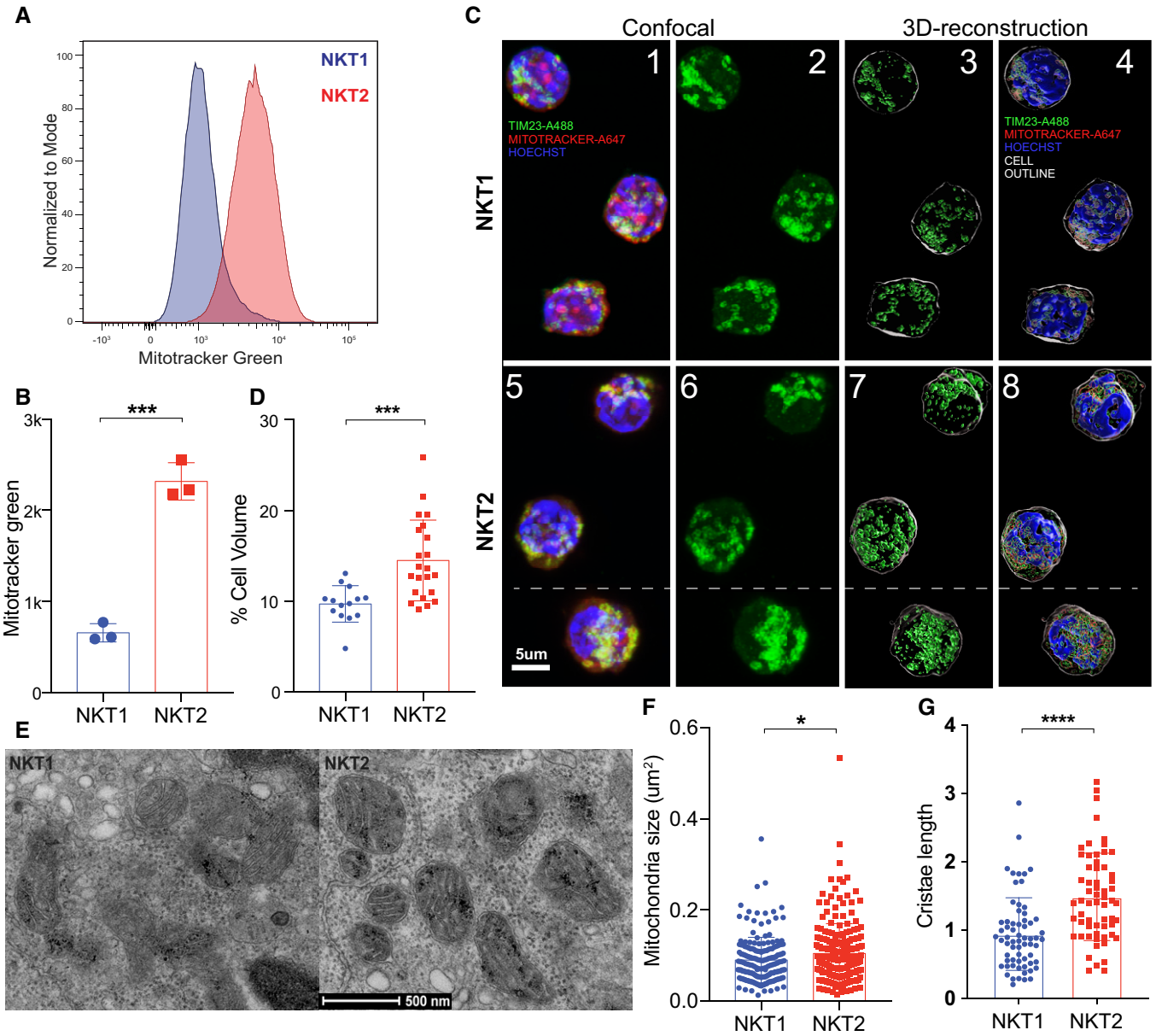

Figure 4. Mitochondria in NKT2 support robust oxidative phosphorylation.

A MitoTracker green staining in iNKT cell subsets *ex vivo*.

B Quantification of mean fluorescence intensity (MFI) of MitoTracker green staining in iNKT cell subsets.

C Confocal images of Tim 23 (Alexa Fluor 488, green) and MitoTracker deep red (Alexa Fluor 647, red) in freshly isolated thymic NKT1 (c1, 2) and NKT2 (c5, 6) cells using Airyscan technology. 3D images reconstructed by Imaris software in NKT1 (c3, 4) and NKT2 cells (c7, 8). Dotted line in panel (5–8) indicates juxtaposition of two NKT2 cell images taken with the same resolution and magnification as NKT1 cells.

D Mitochondrial volume estimated by Tim 23 staining as in (C), and presented as % of total cell volume.

E Representative images of electron microscopy in NKT1 and NKT2 cells.

F, G (F) individual mitochondria size and (G) cristae perimeters normalized to mitochondria perimeter based on EM in (E).

Data information: Data are representative from three independent experiments. Graphs represent mean ± SD with symbols representing individual mice (B), individual cells (D), or individual mitochondrion (F, G). *$P < 0.05$; ***$P < 0.001$; ****$P < 0.0001$; n.s. not significant (unpaired two-tailed Student's *t*-test).

Mitochondria are the major non-ER Ca^{2+} store and have been reported to sequester Ca^{2+} upon Ca^{2+} influx through CRAC channels (Quintana *et al*, 2011). Mitochondrial Ca^{2+} uptake promotes the long-lasting activity of CRAC/ORAI1 channels in human and rat leukemia cell lines (Quintana *et al*, 2011), as well as human primary $CD4^+$ T cells (Quintana *et al*, 2007) by modulating the slow Ca^{2+}-dependent inactivation of CRAC/ORAI channels at the vicinity or microdomain of the channel opening (Schwindling *et al*, 2010). Therefore, we asked whether our findings in NKT2 cells would be consistent with a mechanism in which Ca^{2+} sequestration in

 © 2021 The Authors

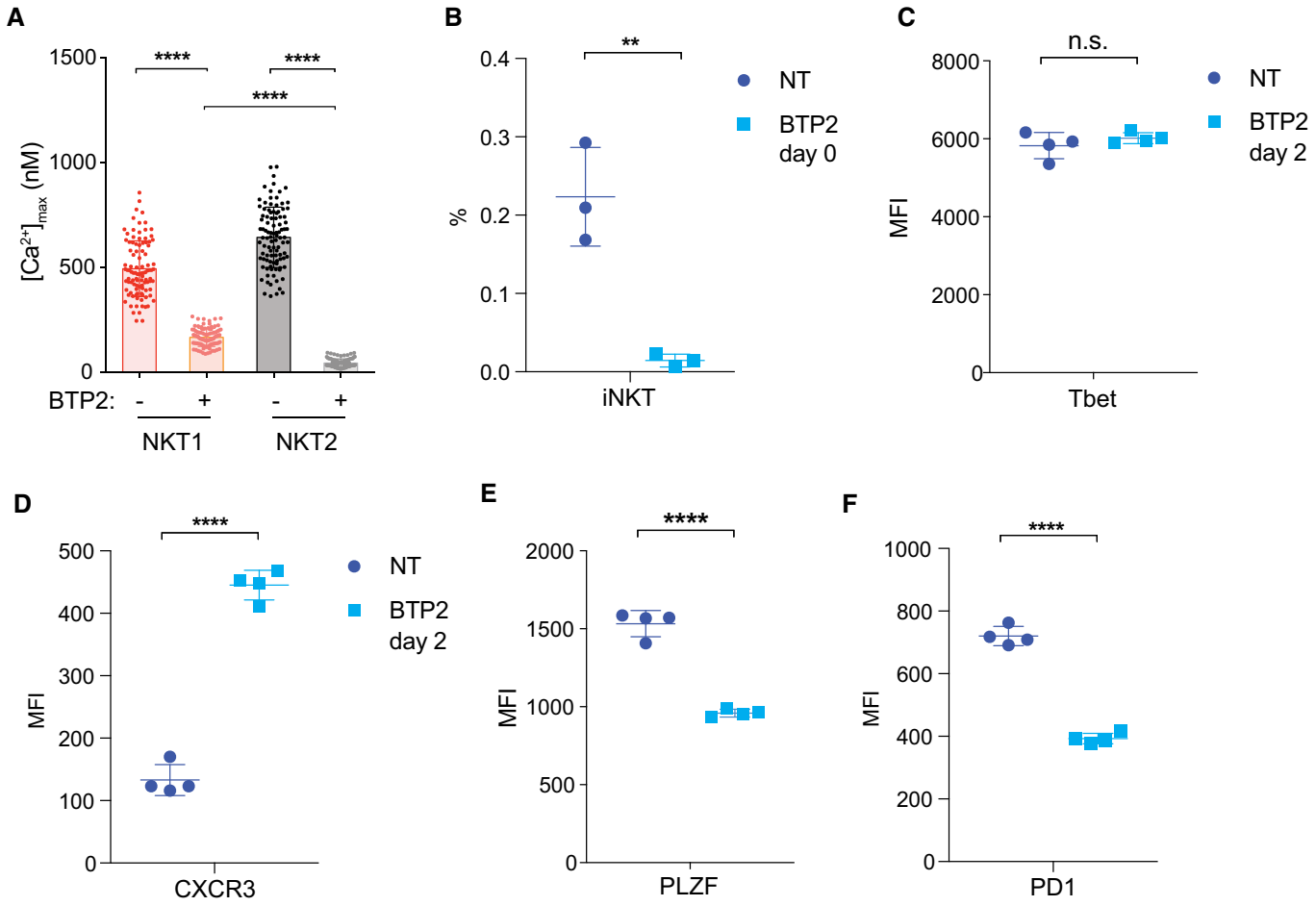

Figure 5. ORAI is required for iNKT cell subset differentiation.

A Maximal cytoplasmic [Ca^{2+}] in single, freshly sorted NKT1 and NKT2 cells following TCR stimulation in the presence or absence of BTP2 (1 μM).

B Percentage of iNKT cells in total live cells in FTOC with or without BTP2 (1 μM) addition at the start of culture (day 0).

C–F BTP2 (1 μM) was added 48 h after the start of culture, and the expression of Tbet (C), CXCR3 (D), PLZF (E), and PD1 (F) in total iNKT cells is shown.

Data information: Data are representative from one of three independent experiments. Graphs represent mean ± SD with symbols representing individual cells (A), or individual thymic lobes (B–F). $^{**}P < 0.01$; $^{****}P < 0.0001$; n.s. not significant (unpaired two-tailed Student's *t*-test).

mitochondria (Fig 6C) contributes to a reduced local Ca^{2+} concentration and Ca^{2+}-dependent CRAC/ORAI inactivation, thereby sustaining the Ca^{2+} entry upon TG treatment and contributing to the high cytoplasmic Ca^{2+} plateau in NKT2 cells after TG (Fig 6A and D). We treated the cells with TG in 0 extracellular Ca^{2+} as in the control (Fig 6A), then applied acutely extracellular Ca^{2+} (0.5 mM) together with the mitochondrial uncoupler CCCP, which abrogates mitochondrial Ca^{2+} uptake by disrupting the mitochondrial membrane potential (Fig 6B). We used lower Ca^{2+} in the perfusion medium (0.5mM), because 1mM Ca^{2+} as in the control condition will lead to saturation of the florescent signals from Fura-2. Although lower extracellular Ca^{2+} affects Ca^{2+} influx in both NKT1 and NKT2 cells, CCCP treatment revealed the role of mitochondria in creating the different Ca^{2+} homeostasis in NKT1 and NKT2 cells (Fig 6A), while still maintaining the dynamic range of the Ca^{2+} signals. As a consequence, the ionomycin peak in both NKT1 and NKT2 cells was diminished, confirming that the increase in cytoplasmic [Ca^{2+}] after ionomycin in the control condition (TG followed by ionomycin, Fig 6A, blue arrow, 6c) was contributed by mitochondrial Ca^{2+}. Importantly, while in the control group NKT2 cells had a higher Ca^{2+} plateau than NKT1 cells, the maximal [Ca^{2+}] was significantly lower in NKT2 cells than in NKT1 cells when CCCP was present (Fig 6D). If Ca^{2+} entry through CRAC/ORAI was maintained during CCCP treatment, inhibition of mitochondrial Ca^{2+} uptake should have increased the level of cytoplasmic [Ca^{2+}]. Instead, our data suggest that mitochondria sequester incoming Ca^{2+} from CRAC/ORAI channels and might help in maintaining the activity of CRAC/ORAI channels, probably through reducing Ca^{2+}-dependent inactivation of the channels. When this important mitochondrial regulation is absent upon CCCP treatment, the increase rate of cytoplasmic Ca^{2+}, which was measured when extracellular Ca^{2+} was applied, was drastically reduced in NKT2 cells as compared to NKT1 cells (Fig 6A,B,E).

The amount of Ca^{2+} sequestered in mitochondria is directly correlated with the level of Ca^{2+} in the cytoplasm as previously reported (Hoth *et al*, 1997; Quintana *et al*, 2011; Quintana & Hoth, 2012). Since NKT2 cells showed a significantly higher Ca^{2+} plateau

© 2021 The Authors

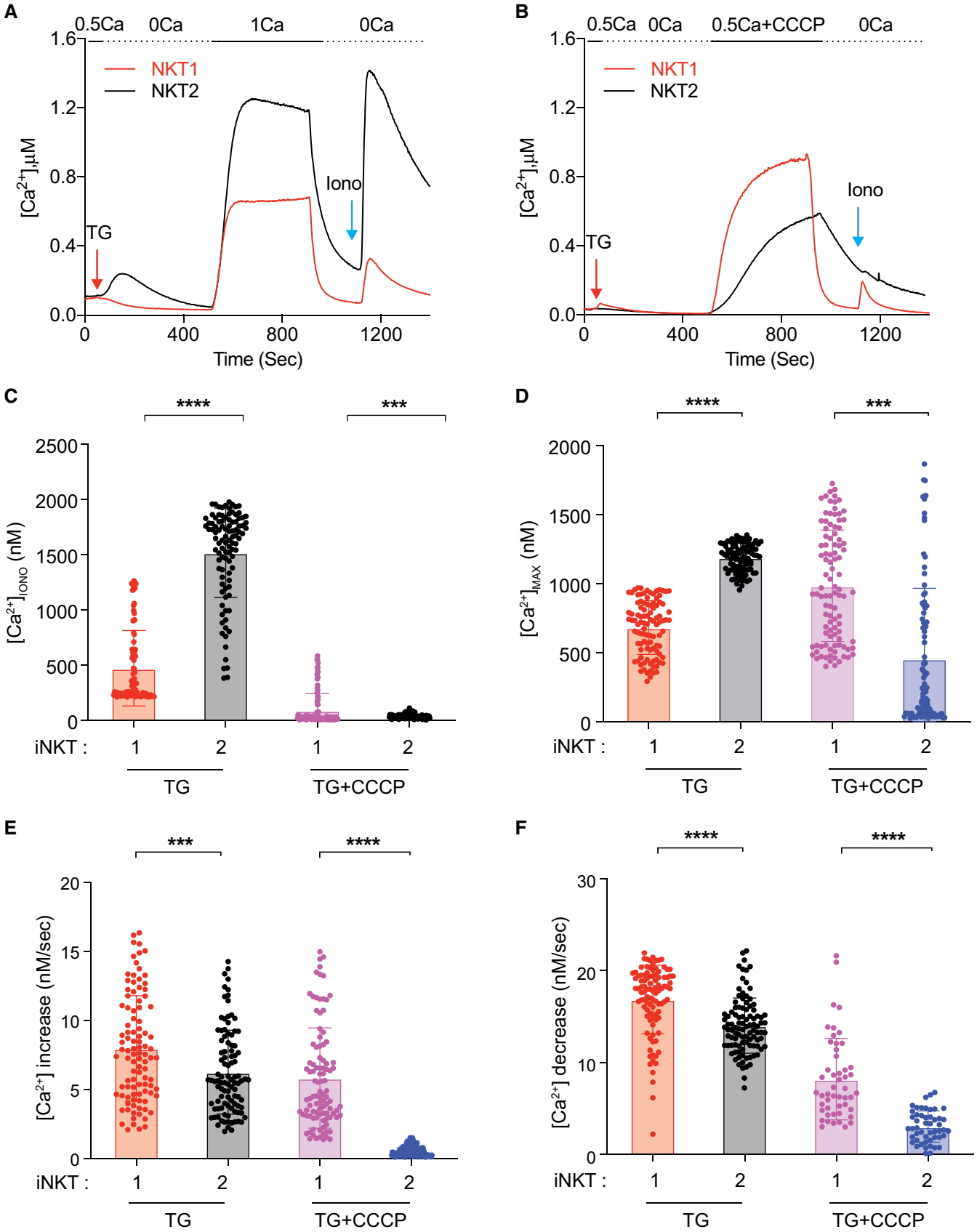

Figure 6.

© 2021 The Authors

Figure 6. Mitochondrial uncoupler differently affects ORAI mediated calcium signals in NKT1 and NKT2 cells.

A, B Profiles showing average Ca^{2+} influx induced by Thapsigargin (TG) in freshly sorted NKT1 (Red) and NKT2 (Black) cells. The timing of TG (1 μM), ionomycin (Iono) (2 μM), and CCCP (1 μM) addition, and extracellular [Ca^{2+}] in mM are shown.

C–F Single-cell quantification related to the data in (A) and (B). (C) cytoplasmic [Ca^{2+}] after ionomycin; (D) maximal cytoplasmic [Ca^{2+}] after TG; (E) increase rate of cytoplasmic [Ca^{2+}] when extracellular Ca^{2+} is applied; (F) decrease rate of cytoplasmic [Ca^{2+}] when extracellular Ca^{2+} is removed in NKT1 and NKT2 cells which have similar Ca^{2+} plateau level (iso-cells; 900–1,200 nM for control group (A), and 400–700 nM for CCCP group (B)).

Data information: Data are representative from one of three independent experiments. Graphs represent the average Ca^{2+} concentration in μM (A, B) or mean ± SD with symbols representing individual cells (C–F). ***$P < 0.001$; ****$P < 0.0001$; (unpaired two-tailed Student's *t*-test).

(Fig 6A), and in order to estimate the real Ca^{2+} sequestration capacity by the mitochondrial network in each cell type, we normalized the ionomycin-induced Ca^{2+} peak to the Ca^{2+} plateau for each individual cell. As shown in Appendix Fig S12, considering the difference in cytoplasmic Ca^{2+} level during TG treatment, the mitochondrial network in NKT2 cells showed a higher capacity to store Ca^{2+} after TG-induced Ca^{2+} influx than NKT1 cells.

The ability of mitochondria to modulate the accumulation of Ca^{2+} near the microdomains and control the Ca^{2+}-dependent channel inactivation is related to the distance between the mitochondria and the plasma membrane, which can be a stand-in for distance between mitochondria and immune synapse/ER-PM junction where CRAC/ORAI channels are located (Hogan, 2015). Quantification of the distance between mitochondria and plasma membrane (PM) based on the confocal imaging of Tim23 (Fig 4C) revealed that mitochondria in NKT2 cells positioned closer to the PM (Appendix Fig S13). Therefore, higher mitochondria content (Fig 4, Appendix Fig S8A and B), the more negative mitochondrial membrane potential (Appendix Fig S8C and D), and the mitochondrial proximity to plasma membrane (Appendix Fig S13) facilitate the mitochondria in NKT2 cells to sequester a large amount of Ca^{2+} in the vicinity of CRAC/ORAI channel and thereby efficiently reducing the Ca^{2+}-dependent channel inactivation.

Ca^{2+} dynamics are generated by the interplay of Ca^{2+} influx and efflux pathways. In addition to Ca^{2+} entry, we asked whether the Ca^{2+} exportation pathways contribute to the higher Ca^{2+} signals observed in NKT2 cells. There are two major systems for Ca^{2+} extrusion, Na^+/Ca^{2+} exchanger (NCX) and the plasma-membrane Ca^{2+} ATPase (PMCA; Brini & Carafoli, 2011). RNA-seq analyses revealed that NCX genes are not expressed in iNKT cells, whereas two isoforms of PMCA, *ATP2b1/Pmca1* and *ATP2b4/Pmca4*, are expressed, and at a significantly higher level in NKT1 than in NKT2 cells, with fold changes of 2.46 and 10.42, respectively (Appendix Fig S14). Therefore, we hypothesized that Ca^{2+} extrusion is less efficient in NKT2 cells than in NKT1 cells, which may contribute to the higher and prolonged Ca^{2+} signals in NKT2 cells after stimulation (Figs 1 A and B and 6A). The activity of PMCA is modulated by the cytosolic Ca^{2+} concentration (Brini & Carafoli, 2011) (Appendix Fig S15). Therefore, PMCA activity should be compared between cells that show the similar Ca^{2+} plateau, so-called iso-cells (Bautista *et al*, 2002; Bautista & Lewis, 2004; Quintana *et al*, 2011; Appendix Fig S15). The Ca^{2+} efflux rate measured within 10 s upon Ca^{2+} removal in cells showing similar plateau [Ca^{2+}] (iso-cells) was significantly faster in NKT1 than in NKT2 cells under control or CCCP conditions (Appendix Fig S15 and Fig 6F). Although these data do not exclude the participation of other potential Ca^{2+} efflux mechanisms, they suggest that the PMCA activity is significantly lower in NTK2 cells compared with NKT1 cells. We propose the low Ca^{2+} extrusion by PMCA significantly contributes to the higher and prolonged Ca^{2+} signals in NKT2 cells, but also highlights the critical role of mitochondria in buffering the incoming Ca^{2+} near the microdomains that control the Ca^{2+}-dependent inactivation of CRAC/ORAI channels.

Compared with CCCP treatment, similar results were observed when cells were treated with antimycin A, which specifically targets complex III of the respiratory chain (bc1-complex) and thereby inhibits the electron transport chain and disrupts the formation of a proton gradient via a distinct mechanism as compared to CCCP. As shown in Appendix Fig S16, antimycin A had a differential effect on the TG-induced Ca^{2+} influx in NKT1 and NKT2 cells, as reflected by the changes in maximal Ca^{2+} concentration ($[Ca^{2+}]_{max}$), and the kinetics of Ca^{2+} influx and efflux. Collectively, we propose that NKT2 cells, compared with NKT1 cells, are more dependent on mitochondria for proper ORAI-mediated Ca^{2+} signaling. Inhibition of mitochondrial Ca^{2+} uptake by either CCCP or antimycin A prohibited Ca^{2+} signaling in NKT2 cells, whereas in NKT1 cells it was minimally affected. Therefore, we identified mitochondria and PMCA as important potential regulators for Ca^{2+} homeostasis in iNKT cell subsets (Fig 7 graphic summary).

Discussion

The functional subsets of iNKT cells are present in different organs of mice at steady state, they maintain tissue homeostasis, influence the microbiome (Brailey *et al*, 2020), and carry out immediate responses during inflammation and infection (Vivier *et al*, 2012; Crosby & Kronenberg, 2018). The subsets of iNKT cells express highly overlapping TCRs (Tuttle *et al*, 2018). Therefore, it is puzzling how the diversification of iNKT cells during differentiation is controlled. In this study, we focused on the two major subsets of iNKT cells: NKT1 and NKT2 cells. We discovered that Ca^{2+} differentially regulated development of these iNKT cell subsets and their responses to TCR activation. Furthermore, CRAC/ORAI-mediated Ca^{2+} signaling is a major control point and is regulated in part by mitochondria.

The differentiation of iNKT cells in vivo is dependent on NF-κB proteins and other factors that are only essential for peripheral CD4 and CD8 immune responses, but not for their differentiation (Engel & Kronenberg, 2014). These additional requirements likely reflect the fact that iNKT cells undergo rounds of expansion in the thymus. Compared with conventional or mainstream $CD4^+$ and $CD8^+$ T cells, we showed that the development of the total iNKT cell population in organ cultures depended on both a higher amount of extracellular Ca^{2+} in the media and optimal activity of CRAC channels (Fig 2). This is in line with the fact that iNKT cells required STIM-ORAI

© 2021 The Authors

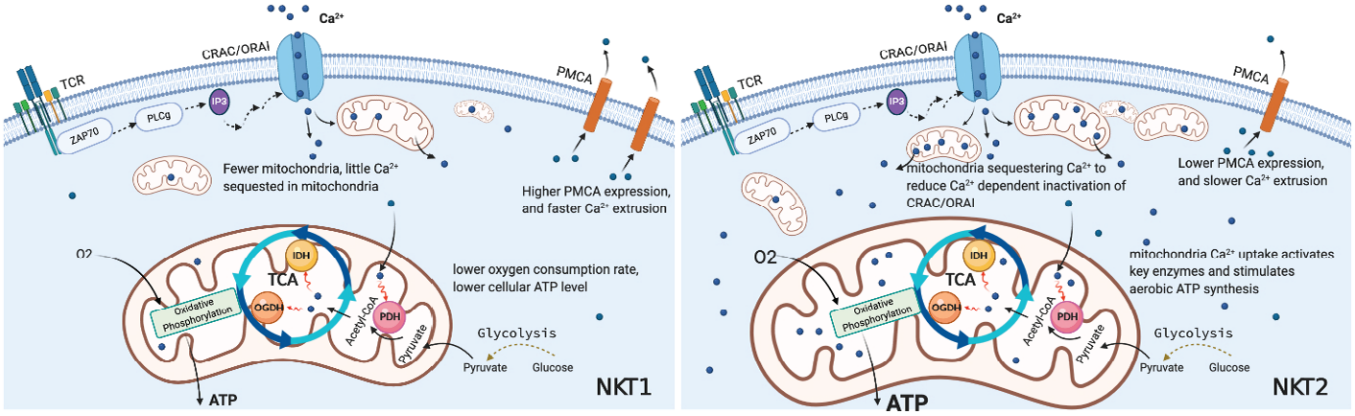

Figure 7. Thymic iNKT cell subsets show distinctive regulation of calcium homeostasis and cellular metabolism.

CRAC/ORAI channel functions down stream of TCR activation, and plays important roles for iNKT cell differentiation and activation. NKT2 cells show higher and prolong Ca^{2+} signals than NKT1 cells after CRAC/ORAI activation. We propose this is regulated by two mechanisms: Mitochondria in NKT2 cells sequester Ca^{2+} at the vicinity of the channel to reduce Ca^{2+}-dependent inactivation of CRAC/ORAI and help maintain the channel activity for Ca^{2+} entry; Lower PMCA expression and slower Ca^{2+} exportation in NKT2 further contribute to higher and sustained Ca^{2+} signals in NKT2 cells. Ca^{2+} in mitochondria is an important co-factor for key metabolic enzymes (PDH: pyruvate dehydrogenase; IDH: isocitrate dehydrogenase; OGDH: 2-oxoglutarate dehydrogenase). Consistently, NKT2 cells show more robust respiration and higher cellular ATP. Note: ER is an important regulator of Ca^{2+} homeostasis and is not shown for purpose of simplicity. Figure was generated using BioRender.

expression in vivo (Oh-Hora *et al*, 2013), and is consistent with the hypothesis that iNKT cells are selected by self-agonists.

Regarding the iNKT cell subsets, NKT2 cells depended on higher TCR signal strength than NKT1 cells, as we and others recently demonstrated using mice expressing mutant ZAP70 (Tuttle *et al*, 2018; Zhao *et al*, 2018). Here, we showed that SKG mice expressing hypomorphic ZAP70 had abnormal TCR-mediated Ca^{2+} flux only in NKT2 cells, with the NKT1 cells unimpaired, consistent with a link between Ca^{2+} homeostasis and iNKT cell subset differentiation (Fig 1). As NKT2 cells also needed more Ca^{2+} for proliferation in vitro (Fig 2), the need for increased and prolonged Ca^{2+} in NKT2 cells could reflect positive selection, TCR-induced proliferation of already committed NKT2 cells, or both. Separating TCR-induced proliferation from positive selection is especially difficult considering iNKT cells. Regardless, the increased requirement for Ca^{2+} in NKT2 cells is clearly established here.

One of the important downstream effects of Ca^{2+} in developing iNKT cells is likely the increased activation of NFAT and Egr proteins, especially as NKT2 cells differentiate. Ca^{2+} is also a critical co-factor for mitochondrial respiration, however, and it stimulates the aerobic synthesis of ATP (Contreras *et al*, 2010). Here, we provide the first in-depth analysis of the metabolism of iNKT cell subsets, and our data indicate that Ca^{2+} can be taken up by mitochondria after activation, and therefore may regulate metabolism during iNKT cell differentiation. Thymic iNKT cell subsets, especially NKT2 cells, maintained a higher level of cellular ATP at steady state and showed higher activity of mitochondrial respiration, as compared with conventional T cells. NKT2 cells also had a high glycolytic potential, although oxidative phosphorylation is the predominant pathway for ATP production in thymic T cells (Appendix Fig S7). The uniquely high metabolic activity in iNKT cells, specifically in NKT2 cells, may reflect the requirement for their thymic differentiation. Consistent with our observation, a recent study showed that deletion of Rieske iron–sulfur protein (RISP), a critical component of ETC complex III, specifically abolished iNKT cell development not conventional T cells, indicating oxidative phosphorylation is essential to drive iNKT cell development (Weng *et al*, 2021). Based on our data, we hypothesize that the differentiation of NKT2 cells may require a higher level of mitochondrial metabolism than NKT1 cells. This should be investigated in the future. Additionally, higher metabolic activity may be required to meet the energetic demand for carrying out homeostatic functions, as iNKT cells are relatively long-lived in the thymus (Kronenberg, 2005). For example, NKT2 cells are a major IL-4 producer at steady state in the thymus, and they influence the development of memory-like $CD8^+$ T cells(Lee *et al*, 2013), $Foxp3^+$ regulatory T cells(Kang *et al*, 2016), and thymic dendritic cells(Lee *et al*, 2013). A recent study suggest that oxidative phosphorylation in total splenic iNKT cells is higher than $CD4^+$ T cells (Kumar *et al*, 2019). We also showed mitochondrial mass in splenic NKT2 cells was higher than in NKT1 cells (Appendix Fig S8E). These data suggest the mechanisms regulating thymic differentiation and the response to TCR-mediated activation may also apply to peripheral iNKT cell subsets, which like their thymic counterparts are mostly not recirculating (Crosby & Kronenberg, 2018).

It has been reported that mitochondria regulate the activity of CRAC/ORAI channel in T cells by modulating the accumulation of Ca^{2+} near the microdomains that control the Ca^{2+}-dependent channel inactivation (Hoth *et al*, 1997; Makowska *et al*, 2000; Quintana *et al*, 2006; Quintana *et al*, 2007; Schwindling *et al*, 2010; Quintana *et al*, 2011; Quintana & Hoth, 2012). It has been proposed that mitochondria do so through either limiting ER Ca^{2+} refilling (Zweifach & Lewis, 1995; Gilabert & Parekh, 2000; Hoth *et al*, 2000) or lowering the local Ca^{2+} concentration near the CRAC channels (Hoth *et al*, 1997; Gilabert & Parekh, 2000; Hoth *et al*, 2000; Hogan, 2015). Mitochondrial Ca^{2+} uptake through the mitochondrial calcium uniporter (MCU; Marchi & Pinton, 2014) is dependent on the high negative mitochondrial membrane potential (−170 mV). The disruption of the mitochondrial membrane potential, by either CCCP or antimycin A treatment, resulted in the block of mitochondrial Ca^{2+} uptake. Subsequently, we observed striking reduction in CRAC-mediated

 © 2021 The Authors

Ca^{2+} influx in NKT2 cells, reflected by both the plateau level and the rate of influx, while the effect in NKT1 was minimal (Fig 6, Appendix Fig S16). These data suggest that mitochondria act as a potent intracellular Ca^{2+} buffer for regulating the Ca^{2+}-dependent ORAI channel inactivation and the subsequent Ca^{2+} signaling in NKT2 cells, with analogy to other T cells as shown previously (Hoth *et al*, 1997; Makowska *et al*, 2000; Quintana *et al*, 2006; Schwindling *et al*, 2010; Quintana *et al*, 2011; Quintana & Hoth, 2012). Therefore, mitochondria may influence NKT2 cell activation and differentiation through regulating Ca^{2+} homeostasis.

In addition to Ca^{2+} entry mechanisms, Ca^{2+} clearance pathways also actively shape the Ca^{2+} homeostasis. Consistent with a major role of Plasma Membrane Ca^{2+} ATPase (PMCA) in the removal of Ca^{2+} in T cells (Lewis, 2001), we found both PMCA1 and PMCA4 are expressed in iNKT cells, whereas genes encoding Na^{+}/Ca^{2+} exchangers (NCXs) are not. Importantly, PMCAs are expressed at significantly higher level in NKT1 than in NKT2 cells, suggesting that Ca^{2+} extrusion in NKT1 cells is more efficient (Appendix Fig S14). When controlling for the difference in the intracellular $[Ca^{2+}]$, we confirmed that the Ca^{2+} efflux rate in NKT1 after TG treatment is significantly higher than in NKT2 cells (Appendix Fig S15). Therefore, PMCAs activity may also potentially affect the Ca^{2+}-dependent cellular function of iNKT cells.

Overall, we propose that Ca^{2+} homeostasis is regulated differently in NKT1 and NKT2 cells. Although the CRAC/ORAI channel is the major Ca^{2+} entry pathway in both NKT1 and NKT2 cells, there may be alternative Ca^{2+} channel(s) functioning in NKT1 cells as evidenced by the residual Ca^{2+} signals upon BTP2 treatment (Fig 5A, Appendix Figs S10 and S11). The identity of this Ca^{2+} channel(s) remains to be defined. Our data suggest that CRAC/ORAI channel activity is positively regulated by mitochondria in NKT2 cells but not in NKT1 cells during activation, likely due to the quantitative and qualitative differences in mitochondria in these two populations as mentioned above. Conceivably, the lack of mitochondria buffering can lead to faster inactivation of CRAC/ORAI in NKT1 cells, which, when combined with faster Ca^{2+} clearance by PMCA, result in lower Ca^{2+} signals during stimulation. On the contrary, mitochondrial buffering to maintain CRAC/ORAI activity, as well as slower Ca^{2+} efflux, may help to sustain higher and prolonged Ca^{2+} signals required for NKT2 cell proliferation and differentiation (Fig 7).

In summary, our study showed the uniquely important role of Ca^{2+} signals downstream of TCR for iNKT cell differentiation compared with mainstream T cells, and distinguishing NKT2 from NKT1 cells. We provided further evidence that ORAI is the critical calcium channel (Oh-Hora *et al*, 2013), and we showed distinct modulation for Ca^{2+} homeostasis involving mitochondria and possibly also PMCA in NKT1 and NKT2 cells. Overall, our data provide new insights into the regulatory mechanisms of iNKT cell differentiation leading to the acquisition of different effector functions with implications for understanding the acquisition of natural type 2 immunity.

Materials and Methods

Mice

BALB/cJ and C57BL6/J were from Jackson Laboratories. SKG mice were obtained from S. Sakaguchi (Osaka University) via N. Bottini (UC-San Diego). Mice were bred and housed at the La Jolla Institute for Immunology (LJI) vivarium and Oklahoma Medical Research Foundation (OMRF) vivarium under specific pathogen-free conditions (SPF). All experiments were conducted in accordance with the protocols approved by the Institutional Animal Care and Use Committee of LJI and OMRF.

Flow cytometry and antibodies

Single-cell suspensions were prepared from thymus. Before antibody staining, cells were pre-incubated with Fc block (BD Biosciences). CD1d-αGalCer tetramers were prepared in our laboratory as described previously (Sidobre & Kronenberg, 2002) or were obtained from the NIH Tetramer Facility, and used at a dilution of 1:200. Staining for transcription factors was performed using reagents and protocols from the Transcription Factor (TF) Buffer Set (BD Biosciences). The complete list of other antibodies and reagents used is as follows: Live/Dead-Yellow (Thermo Fisher), anti-TCRβ (H57-597), anti-CD4 (RM4-5), anti-CD8α (53-6.7), anti-CD19 (6D5), anti-CD24 (M1/69), anti-CD44 (IM7) and anti-NK1.1 (PK136), anti-CXCR3 (CXCR3-173), anti-CD49A (Ha31/8), anti-CD122(TM-beta1), anti-CD5(53-7.3), anti-PD-1(29F.1A12), anti-ICOS (C398.4A), anti-FR4(12A5), anti-Slamf6(330AJ), anti-Sdc-1(281-2), anti-TOM20 (D8T4N), anti-TIM23(32/Tim23), anti-TOM22(ab57523), anti-PLZF (R17-809), anti-T-bet (O4-46), and anti-RORγt (Q31-378 or B2D). Stained samples are analyzed using either LSRII or Fortessa flow cytometers (BD Biosciences) and FlowJo software (Treestar), or using microscopy as detailed below.

Pre-enrichment and isolation of thymic iNKT cell subsets

Thymic iNKT cells were negatively enriched from total thymocytes by using ani-CD8α, CD24, CD19, and Ter119. For iNKT cell subset sorting by FACS, pre-enriched thymocytes were stained with TCRβ, CD1d-αGalCer tetramers, ICOS, CD49a, and CD4. NKT1 cells were $TCR\beta^{int}$,CD1d-αGalCer $tetramer^{+}ICOS^{lo}CD49a^{+}$, and NKT2 cells were $TCR\beta^{int}$,CD1d-αGalCer $tetramer^{+}ICOS^{hi}CD4^{+}Sdc1^{-}$. Sdc1 was used to select against IL-17-producing NKT17 cells (Dai *et al*, 2015). Subsets verified by transcription factors staining as shown in (Zhao *et al*, 2018).

In vitro iNKT cell proliferation

Flow-sorted iNKT cell subsets were stained with Cell Trace Violet dye and cultured in vitro with anti-CD3ε/CD28 Dynabeads at 4×10^4 cells/1ul beads in complete DMEM medium supplemented with IL-7 (5 ng/ml) and IL-15/IL15Ra (5 ng/ml, Thermo Fisher) for 2 days. Cell division index is calculated based on Cell Trace Violet signal using FlowJo software (Treestar).

Calcium flux assay

As described (Fu & Gascoigne, 2009), thymocytes from WT mice pre-enriched for iNKT cells (see above) were labeled with CFSE (20 nM) in PBS for 10 min at 37°C, washed, and mixed with thymocytes from SKG mice ($CSFE^{neg}$) at a 1:1 ratio. Cells were then loaded with a 2 μM concentration of Indo-1 AM (Thermo Fisher) with 4 μM probenecid (Thermo Fisher) in RPMI with 1% FBS. After

© 2021 The Authors

washing, cells were stained with CD1d-αGalCer tetramers and antibodies against TCRβ, CD4, and ICOS. For TCR activation-induced Ca^{2+} influx measurement, cells were also stained with purified hamster anti-mouse CD3ε antibodies (10 ug/ml, 145-2C11; BioLegend) on ice. Cells were resuspended in PBS, and goat anti-Armenian hamster IgG (H + L) (Jackson Immuno Research) was used as a cross-linker. For Thapsigargin (TG)-induced Ca^{2+} influx, cells were incubated with TG (1 μM) in PBS while baseline calcium signal was recorded. Calcium flux was initiated after addition of $CaCl_2$ (1mM). The mean fluorescence ratio of Indo-1 violet to Indo-1 blue was calculated using FlowJo software (Tree Star, Inc.).

Thymic organ culture

Timed breedings were set up and thymic lobes were harvested from e18.5 embryos or d0 mice. Lobes were cultured on cell culture inserts with 0.4 μm pore in 6-well culture dishes (Sigma #CLS3450) on top of 1.6 ml complete DMEM supplemented with 10% FBS. Medium was exchanged daily until thymic lobes were dissociated into single-cell suspensions for staining with antibodies for flow cytometric analysis.

Compounds and reagents

MitoTracker Green and TMRE were from Thermo Fisher. EGTA solution was from BioWorld. BTP2, Thapsigargin, and CCCP were from Tocris. Oligomycin, DNP, and Myxothiazol were from Sigma. CellTiter-Glo Luminescent ATP assay kit was from Promega.

Single-cell Ca^{2+} imaging

Sorted iNKT cells were loaded with 1–2 μM Fura-2/AM in RPMI-1640 medium supplemented with 10mM HEPES and 0.1% Pluronic F-127 (PF-127, Sigma). After 20 min, cells were washed twice in RPMI-1640 medium and then immobilized on 10 ug/ml poly-ornithine coated 18 mm coverslips. Olympus IX 71 microscope equipped with an Olympus UPLSAPO ×20, numerical aperture (NA) 0.75 objective was used for the Ca^{2+} influx assays. Cells were alternately illuminated at 340 and 380 nm with the polychrome V monochromator (TILL Photonics) using an ET FURA2 filter set (Chroma Technology Corp). The fluorescence emission at $\lambda > 400$ nm (T400lp dichroic beamsplitter, ET510/80m emission filter) was captured with a CCD camera (SensiCam, TILL Imago), digitized, and analyzed by TILL Vision software. Ratio images were recorded at intervals of 2s. Ca^{2+} concentration was estimated from the relation: $[Ca^{2+}]_i = K \times (R-R_{min})/(R_{max}-R)$, in which the values of K, R_{min}, and R_{max} were determined from an in situ calibration of Fura-2 in iNKT cells.

During the recorded imaging time, cells were first washed with modified 0.5 mM Ca^{2+} Ringer's solution (mM): 20 HEPES, 125 NaCl, 5 KCl, 2 $MgCl_2$, 0.5 $CaCl_2$, 10 D-glucose (pH 7.4 with NaOH). Antibody stimulation was achieved by using an anti-CD3ε + anti-CD28 mAb (5 μg/ml) mixture. ER Ca^{2+} store depletion was achieved by perfusion with 1 μM TG in 1 mM EDTA containing Ringer's solution. For control cells, 1 mM Ca^{2+} Ringer buffer (mM): 20 HEPES, 125 NaCl, 5KCl, 1.5 $MgCl_2$, 1.0 $CaCl_2$, and 10 D-glucose was used for initiating Ca^{2+} influx. For drug treatment groups, cells were either treated with 1 μM CCCP or 1 μM antimycin in the presence of 0.5 mM Ca^{2+} Ringer buffer. For BTP2 treatment, cells were pretreated with BTP2 (1 μM) for 30 min before the recording. Data were analyzed using TILL vision (TILL Photonics) and Igor Pro (WaveMetrics).

LSM confocal microscopy and analysis

All images were acquired in Airscan mode on a Zeiss LSM 880 Airyscan Confocal Microscopy (Zeiss Inc.) as z stacks using a 63× (1.46na) objective, at 0.18 μm step sizes (nyquist optimal settings). Following acquisition using a module within the Zeiss Zen software (Zeiss, Inc.), all z stacks of each image were auto-post processed by the Zen software as a Sheppard Sum image and deconvolved into the final super-resolved and corrected image prior to importing into IMARIS software (Bitplane Inc.) for 3D analysis of mitochondrial and whole-cell volume rendering. To define the 3D spatial localization of mitochondria, the TIM23 fluorescent signal was iso-surfaced and rendered as numerous 3-dimensional regions of interest (ROI). To define the whole-cell periphery (plasma membrane), the WGA and/or autofluorescence signal was used to render a 3D cell outline ROI. Both mitochondrial ROIs and whole-cell ROIs were imported into the Imaris Cell module where the software automatically calculated the closest (um) distances between the mitochondrial iso-surfaced membranes and the cell periphery or plasma membrane and the results were exported into excel.

Super-resolution STORM imaging

As outlined in Fan *et al* (2019), images were captured using 100× 1.49 NA Apo TIRF objective either with TIRF illumination on a Nikon Ti super-resolution microscope. Images were collected on an ANDOR IXON3 Ultra DU897 EMCCD camera using the multicolor sequential mode setting in the NIS-Elements AR software (Nikon Instruments Inc., NY). Power on the 488-, 561-, and 647-nm lasers was adjusted to 50% to enable collection of between 100 and 300 molecules per 256 × 256 camera pixel frame in the center of the field at appropriate threshold settings for each channel. Collection was set to 20,000 frames, yielding 1–2 million molecules, and the super-resolution images were reconstructed with the Nikon STORM software. Positions of individual molecules have been localized with high accuracy by switching them on and off sequentially using the 488-, 561-, and 647-nm lasers at appropriate power settings. The positions determined from multiple switching cycles can show a substantial drift over the duration of the acquisition. This error is considerably reduced by calculating and correcting for sample drift over the course of the experiment by an auto-correlation method used by the Nikon software. This is done by correlating STORM images reconstructed from 200 to 1,000 frames to that from the beginning of the acquisition (Fan *et al*, 2019). The number of frames used in a set is based on the number of molecules identified, and by default, this is set to 10,000 molecules. Displacement is corrected by translational displacement in the X, Y direction for 2D STORM. Axial drift over the course of the acquisition is minimized by engaging the Nikon perfect focus system. Calibration of chromatic shift (warp correction) was carried out using a multicolored 100 nm TetraSpeck beads using minimum density per field of over 100 beads. Calibration for warp correction for 2D STORM was executed using the 2D warp calibration feature of the Nikon STORM software. Briefly, a

 © 2021 The Authors

total of 201 images were collected for each of the color channels (488, 561, and 647 nm) without the cylindrical lens in place. Frames 1–20 and frames 182–201 are collected at the focal position. Frames 21–181 are collected across a range of 1.6 microns in 10 nm steps in the Z (covering 800 nm above and 800 nm below the focal plane). The calibration files generated from this macro (software feature) were applied during analysis for the correction of the STORM images. Blinking events were followed for successive frames to ensure single molecule isolation by filtering out molecules with traces longer than 5 frames during analysis. Moreover, individual molecules were localized using point spread function (PSF) width filters of 200–400 nm based on a 100× 1.49 objective and restrictions were placed on photon count signals associated with camera noise of the ANDOR EMCCD (estimated at 100 intensity units above 0). The data were further filtered based on empirical observation of photon count signals (peak height when converted to an intensity value) found in cells vs background staining on the glass slide surface (generally values above 300–700 intensity units above camera noise). The precision of the localization during a switching cycle is calculated from these multiple parameters and from photon counts using molecules that are ultimately well separated in the sample itself (Rust *et al*, 2006; Huang *et al*, 2008; Fan *et al*, 2019).

Electron microscopy

Freshly sorted iNKT cell subsets were immediately fixed. Sample processing was carried out by the UCSD Electron Microscopy Core Facility. Mitochondrial morphology was visualized by transmission electron microscopy. Mitochondrial size and cristae length were quantified using Fiji ImageJ software.

Seahorse metabolic assay

Flow-sorted iNKT cell subsets were washed with Seahorse assay buffer (DMEM with 1 mM pyruvate, 2 mM glutamine, and 10 mM glucose, pH 7.4), and seeded in XF96 well microplate coated with CellTek at 3×10^5/well. The plate was spun at 500 g for 5 min to attach the cells to the bottom of the wells. When measuring glycolysis, glucose-free buffer was used (see Appendix Figs S6 and S7). Standard procedures were followed according to Agilent Seahorse XF Cell Mito Stress test protocol using Seahorse XFe96 bioanalyzer (Agilent Technologies).

Data availability

RNA-seq data in this study have been deposited in GEO with the accession codes GSE114555 (http://www.ncbi.nlm.nih.gov/geo/query/acc.cgi?acc=GSE114555). Other data that support the findings of this study are available from the corresponding authors upon reasonable request.

Expanded View for this article is available online.

Acknowledgments
We thank C. Kim, L. Nosworthy, D. Hinz, and R. Simmons for assisting with iNKT cell subset sorting. Sara McArdle for assisting with EM data analysis; Ashu Sethi for assisting with RNA-Seq data analysis; S. Sakaguchi (Osaka University) for SKG mice; and A. Khurana and Y. Kushnareva for technical assistance. The study is supported by the US National Institutes of Health (NIH) AI71922 and AI137230 to M.K., AI084167 and AI040127 to P.G.H, T32 AR064194 fellowship, P30AR073761 pilot grant, P30AR073750 pilot grant, Presbyterian Health Foundation biomedical research grant, P20GM139763 to M.Z., and NIH instrument grants S10OD021831 (Zeiss LSM 880), S10OD016262 (Illumina HiSeq 2500), S10RR027366 (BD FACSAria II), and S10OD028479 (Cytek Aurora analyzer).

Author contributions
Design and experiments: MZ, AQ, CZ, and AYA; Analysis of the imaging results: WK; Data analysis: TK and AM; Manuscript writing: MZ, AQ, AYA, CZ, PGH, and MK; Study supervision: MZ, PGH, and MK.

Conflict of interest
The authors declare that they have no conflict of interest.

References

Bailey S, Macardle PJ (2006) A flow cytometric comparison of Indo-1 to fluo-3 and Fura Red excited with low power lasers for detecting Ca(2+) flux. *J Immunol Methods* 311: 220 – 225

Baldwin TA, Hogquist KA, Jameson SC (2004) The fourth way? Harnessing aggressive tendencies in the thymus. *J Immunol* 173: 6515 – 6520

Bautista DM, Hoth M, Lewis RS (2002) Enhancement of calcium signalling dynamics and stability by delayed modulation of the plasma-membrane calcium-ATPase in human T cells. *J Physiol* 541: 877 – 894

Bautista DM, Lewis RS (2004) Modulation of plasma membrane calcium-ATPase activity by local calcium microdomains near CRAC channels in human T cells. *J Physiol* 556: 805 – 817

Bird GS, Putney Jr JW (2018) Pharmacology of store-operated calcium entry channels. In *Calcium Entry Channels in Non-Excitable Cells*, Kozak JA, Putney JW (eds), pp 311 – 324. Boca Raton, FL: CRC Press/Taylor & Francis

Brailey PM, Lebrusant-Fernandez M, Barral P (2020) NKT cells and the regulation of intestinal immunity: a two-way street. *FEBS J* 287: 1686 – 1699

Brennan PJ, Brigl M, Brenner MB (2013) Invariant natural killer T cells: an innate activation scheme linked to diverse effector functions. *Nat Rev Immunol* 13: 101 – 117

Brini M, Carafoli E (2011) The plasma membrane Ca2+ ATPase and the plasma membrane sodium calcium exchanger cooperate in the regulation of cell calcium. *Cold Spring Harbor Perspect Biol* 3: a004168

Cheroutre H, Mucida D, Lambolez F (2009) The importance of being earnestly selfish. *Nat Immunol* 10: 1047 – 1049

Contreras L, Drago I, Zampese E, Pozzan T (2010) Mitochondria: the calcium connection. *Biochem Biophys Acta* 1797: 607 – 618

Courtney AH, Lo WL, Weiss A (2018) TCR signaling: mechanisms of initiation and propagation. *Trends Biochem Sci* 43: 108 – 123

Crosby CM, Kronenberg M (2018) Tissue-specific functions of invariant natural killer T cells. *Nat Rev Immunol* 18: 559 – 574

Dai H, Rahman A, Saxena A, Jaiswal AK, Mohamood A, Ramirez L, Noel S, Rabb H, Jie C, Hamad AR (2015) Syndecan-1 identifies and controls the frequency of IL-17-producing naive natural killer T (NKT17) cells in mice. *Eur J Immunol* 45: 3045 – 3051

Engel I, Kronenberg M (2014) Transcriptional control of the development and function of Valpha14i NKT cells. *Curr Top Microbiol Immunol* 381: 51 – 81

Engel I, Seumois G, Chavez L, Samaniego-Castruita D, White B, Chawla A, Mock D, Vijayanand P, Kronenberg M (2016) Innate-like functions of

© 2021 The Authors

natural killer T cell subsets result from highly divergent gene programs. *Nat Immunol* 17: 728 – 739

Fan Z, Kiosses WB, Sun H, Orecchioni M, Ghosheh Y, Zajonc DM, Arnaout MA, Gutierrez E, Groisman A, Ginsberg MH *et al* (2019) High-affinity bent beta2-integrin molecules in arresting neutrophils face each other through binding to ICAMs in cis. *Cell Rep* 26: 119 – 130

Fu G, Gascoigne NR (2009) Multiplexed labeling of samples with cell tracking dyes facilitates rapid and accurate internally controlled calcium flux measurement by flow cytometry. *J Immunol Methods* 350: 194 – 199

Georgiev H, Ravens I, Benarafa C, Forster R, Bernhardt G (2016) Distinct gene expression patterns correlate with developmental and functional traits of iNKT subsets. *Nat Commun* 7: 13116

Gilabert JA, Parekh AB (2000) Respiring mitochondria determine the pattern of activation and inactivation of the store-operated Ca(2+) current I (CRAC). *EMBO J* 19: 6401 – 6407

Godfrey DI, Stankovic S, Baxter AG (2010) Raising the NKT cell family. *Nat Immunol* 11: 197 – 206

Grynkiewicz G, Poenie M, Tsien RY (1985) A new generation of Ca^{2+} indicators with greatly improved fluorescence properties. *J Biol Chem* 260: 3440 – 3450

He LP, Hewavitharana T, Soboloff J, Spassova MA, Gill DL (2005) A functional link between store-operated and TRPC channels revealed by the 3,5-bis (trifluoromethyl)pyrazole derivative, BTP2. *J Biol Chem* 280: 10997 – 11006

Hogan PG (2015) The STIM1-ORAI1 microdomain. *Cell Calcium* 58: 357 – 367

Hogan PG, Rao A (2015) Store-operated calcium entry: mechanisms and modulation. *Biochem Biophys Res Comm* 460: 40 – 49

Hoth M, Button DC, Lewis RS (2000) Mitochondrial control of calcium-channel gating: a mechanism for sustained signaling and transcriptional activation in T lymphocytes. *Proc Natl Acad Sci USA* 97: 10607 – 10612

Hoth M, Fanger CM, Lewis RS (1997) Mitochondrial regulation of store-operated calcium signaling in T lymphocytes. *J Cell Biol* 137: 633 – 648

Huang B, Wang W, Bates M, Zhuang X (2008) Three-dimensional super-resolution imaging by stochastic optical reconstruction microscopy. *Science* 319: 810 – 813

Johnston IG, Williams BP (2016) Evolutionary inference across eukaryotes identifies specific pressures favoring mitochondrial gene retention. *Cell Syst* 2: 101 – 111

Kang BH, Park HJ, Park HJ, Lee JI, Park SH, Jung KC (2016) PLZF(+) Innate T cells support the TGF-beta-dependent generation of activated/memory-like regulatory T cells. *Mol Cells* 39: 468 – 476

Kovalovsky D, Uche OU, Eladad S, Hobbs RM, Yi W, Alonzo E, Chua K, Eidson M, Kim H-J, Im JS *et al* (2008) The BTB-zinc finger transcriptional regulator PLZF controls the development of invariant natural killer T cell effector functions. *Nat Immunol* 9: 1055 – 1064

Kronenberg M (2005) Toward an understanding of NKT cell biology: progress and paradoxes. *Annu Rev Immunol* 23: 877 – 900

Krovi SH, Gapin L (2018) Invariant natural killer T cell subsets-more than just developmental intermediates. *Front Immunol* 9: 1393

Kumar A, Pyaram K, Yarosz EL, Hong H, Lyssiotis CA, Giri S, Chang CH (2019) Enhanced oxidative phosphorylation in NKT cells is essential for their survival and function. *Proc Natl Acad Sci USA* 116: 7439 – 7448

Lazarevic V, Zullo AJ, Schweitzer MN, Staton TL, Gallo EM, Crabtree GR, Glimcher LH (2009) The gene encoding early growth response 2, a target of the transcription factor NFAT, is required for the development and maturation of natural killer T cells. *Nat Immunol* 10: 306 – 313

Lee YJ, Holzapfel KL, Zhu J, Jameson SC, Hogquist KA (2013) Steady-state production of IL-4 modulates immunity in mouse strains and is determined by lineage diversity of iNKT cells. *Nat Immunol* 14: 1146 – 1154

Lee YJ, Starrett GJ, Lee ST, Yang R, Henzler CM, Jameson SC, Hogquist KA (2016) Lineage-specific effector signatures of invariant NKT cells are shared amongst gammadelta T, innate lymphoid, and Th cells. *J Immunol* 197: 1460 – 1470

Lewis RS (2001) Calcium signaling mechanisms in T lymphocytes. *Annu Rev Immunol* 19: 497 – 521

Makowska A, Zablocki K, Duszynski J (2000) The role of mitochondria in the regulation of calcium influx into Jurkat cells. *Eur J Biochem* 267: 877 – 884

Marchi S, Pinton P (2014) The mitochondrial calcium uniporter complex: molecular components, structure and physiopathological implications. *J Physiol* 592: 829 – 839

Miller CN, Proekt I, von Moltke J, Wells KL, Rajpurkar AR, Wang H, Rattay K, Khan IS, Metzger TC, Pollack JL *et al* (2018) Thymic tuft cells promote an IL-4-enriched medulla and shape thymocyte development. *Nature* 559: 627 – 631

Moran AE, Holzapfel KL, Xing Y, Cunningham NR, Maltzman JS, Punt J, Hogquist KA (2011) T cell receptor signal strength in Treg and iNKT cell development demonstrated by a novel fluorescent reporter mouse. *J Exp Med* 208: 1279 – 1289

Mycko MP, Ferrero I, Wilson A, Jiang W, Bianchi T, Trumpp A, MacDonald HR (2009) Selective requirement for c-Myc at an early stage of V(alpha)14i NKT cell development. *J Immunol* 182: 4641 – 4648

Oh-Hora M, Komatsu N, Pishyareh M, Feske S, Hori S, Taniguchi M, Rao A, Takayanagi H (2013) Agonist-selected T cell development requires strong T cell receptor signaling and store-operated calcium entry. *Immunity* 38: 881 – 895

Ong HL, Subedi KP, Son GY, Liu X, Ambudkar IS (2019) Tuning store-operated calcium entry to modulate Ca(2+)-dependent physiological processes. *Biochim Biophys Acta Mol Cell Res* 1866: 1037 – 1045

Pearce EL, Poffenberger MC, Chang CH, Jones RG (2013) Fueling immunity: insights into metabolism and lymphocyte function. *Science* 342: 1242454

Pfanner N, Warscheid B, Wiedemann N (2019) Mitochondrial proteins: from biogenesis to functional networks. *Nat Rev Mol Cell Biol* 20: 267 – 284

Prakriya M, Feske S, Gwack Y, Srikanth S, Rao A, Hogan PG (2006) Orai1 is an essential pore subunit of the CRAC channel. *Nature* 443: 230 – 233

Prevot N, Pyaram K, Bischoff E, Sen JM, Powell JD, Chang CH (2015) Mammalian target of rapamycin complex 2 regulates invariant NKT cell development and function independent of promyelocytic leukemia zinc-finger. *J Immunol* 194: 223 – 230

Quintana A, Hoth M (2012) Mitochondrial dynamics and their impact on T cell function. *Cell Calcium* 52: 57 – 63

Quintana A, Pasche M, Junker C, Al-Ansary D, Rieger H, Kummerow C, Nuñez L, Villalobos C, Meraner P, Becherer U *et al* (2011) Calcium microdomains at the immunological synapse: how ORAI channels, mitochondria and calcium pumps generate local calcium signals for efficient T-cell activation. *EMBO J* 30: 3895 – 3912

Quintana A, Schwarz EC, Schwindling C, Lipp P, Kaestner L, Hoth M (2006) Sustained activity of calcium release-activated calcium channels requires translocation of mitochondria to the plasma membrane. *J Biol Chem* 281: 40302 – 40309

Quintana A, Schwindling C, Wenning AS, Becherer U, Rettig J, Schwarz EC, Hoth M (2007) T cell activation requires mitochondrial translocation to the immunological synapse. *Proc Natl Acad Sci USA* 104: 14418 – 14423

Rengarajan J, Mittelstadt PR, Mages HW, Gerth AJ, Kroczek RA, Ashwell JD, Glimcher LH (2000) Sequential involvement of NFAT and Egr transcription factors in FasL regulation. *Immunity* 12: 293 – 300

Rodrigues MA, Gomes DA, Leite MF, Grant W, Zhang L, Lam W, Cheng YC, Bennett AM, Nathanson MH (2007) Nucleoplasmic calcium is required for cell proliferation. *J Biol Chem* 282: 17061 – 17068

 © 2021 The Authors

Rust MJ, Bates M, Zhuang X (2006) Sub-diffraction-limit imaging by stochastic optical reconstruction microscopy (STORM). *Nat Methods* 3: 793 – 795

Salio M, Silk JD, Jones EY, Cerundolo V (2014) Biology of CD1- and MR1-restricted T cells. *Annu Rev Immunol* 32: 323 – 366

Savage AK, Constantinides MG, Han J, Picard D, Martin E, Li B, Lantz O, Bendelac A (2008) The transcription factor PLZF directs the effector program of the NKT cell lineage. *Immunity* 29: 391 – 403

Schwindling C, Quintana A, Krause E, Hoth M (2010) Mitochondria positioning controls local calcium influx in T cells. *J Immunol* 184: 184 – 190

Seiler MP, Mathew R, Liszewski MK, Spooner CJ, Barr K, Meng F, Singh H, Bendelac A (2012) Elevated and sustained expression of the transcription factors Egr1 and Egr2 controls NKT lineage differentiation in response to TCR signaling. *Nat Immunol* 13: 264 – 271

Shao H, Kono DH, Chen LY, Rubin EM, Kaye J (1997) Induction of the early growth response (Egr) family of transcription factors during thymic selection. *J Exp Med* 185: 731 – 744

Sharma S, Quintana A, Findlay GM, Mettlen M, Baust B, Jain M, Nilsson R, Rao A, Hogan PG (2013) An siRNA screen for NFAT activation identifies septins as coordinators of store-operated Ca^{2+} entry. *Nature* 499: 238 – 242

Sidobre S, Kronenberg M (2002) CD1 tetramers: a powerful tool for the analysis of glycolipid-reactive T cells. *J Immunol Methods* 268: 107 – 121

Steinckwich N, Frippiat JP, Stasia MJ, Erard M, Boxio R, Tankosic C, Doignon I, Nusse O (2007) Potent inhibition of store-operated Ca2+ influx and superoxide production in HL60 cells and polymorphonuclear neutrophils by the pyrazole derivative BTP2. *J Leukoc Biol* 81: 1054 – 1064

Tuttle KD, Krovi SH, Zhang J, Bedel R, Harmacek L, Peterson LK, Dragone LL, Lefferts A, Halluszczak C, Riemondy K *et al* (2018) TCR signal strength controls thymic differentiation of iNKT cell subsets. *Nat Commun* 9: 2650

Vaeth M, Kahlfuss S, Feske S (2020) CRAC channels and calcium signaling in T cell-mediated immunity. *Trends Immunol* 41: 878 – 901

Vivier E, Ugolini S, Blaise D, Chabannon C, Brossay L (2012) Targeting natural killer cells and natural killer T cells in cancer. *Nat Rev Immunol* 12: 239 – 252

Wang Y, Sedimbi S, Lofbom L, Singh AK, Porcelli SA, Cardell SL (2018) Unique invariant natural killer T cells promote intestinal polyps by suppressing TH1 immunity and promoting regulatory T cells. *Mucosal Immunol* 11: 131 – 143

Weng X, Kumar A, Cao L, He Y, Morgun E, Visvabharathy L, Zhao J, Sena LA, Weinberg SE, Chandel NS *et al* (2021) Mitochondrial metabolism is essential for invariant natural killer T cell development and function. *Proc Natl Acad Sci USA* 118: e2021385118

van der Windt GJ, Pearce EL (2012) Metabolic switching and fuel choice during T-cell differentiation and memory development. *Immunol Rev* 249: 27 – 42

Zhang L, Tschumi BO, Corgnac S, Ruegg MA, Hall MN, Mach JP, Romero P, Donda A (2014) Mammalian target of rapamycin complex 1 orchestrates invariant NKT cell differentiation and effector function. *J Immunol* 193: 1759 – 1765

Zhao M, Svensson MND, Venken K, Chawla A, Liang S, Engel I, Mydel P, Day J, Elewaut D, Bottini N *et al* (2018) Altered thymic differentiation and modulation of arthritis by invariant NKT cells expressing mutant ZAP70. *Nat Commun* 9: 2627

Zitt C, Strauss B, Schwarz EC, Spaeth N, Rast G, Hatzelmann A, Hoth M (2004) Potent inhibition of Ca2+ release-activated Ca2+ channels and T-lymphocyte activation by the pyrazole derivative BTP2. *J Biol Chem* 279: 12427 – 12437

Zweifach A, Lewis RS (1995) Slow calcium-dependent inactivation of depletion-activated calcium current. Store-dependent and -independent mechanisms. *J Biol Chem* 270: 14445 – 14451

© 2021 The Authors